Anonymous Referee #1 comments and response

We would like to thank the reviewer very much for the time and effort put into reviewing our manuscript. A point-by-point reply (in blue) to each comment (in black) by Referee #1 are given below. Specific changes in the manuscript are written in blue italics.

Summary:
This manuscript proposes a new method to couple the Full Stokes and Shelfy Stream Approximations so that different parts of a model domain can rely on different approximations of the stress balance equations. The idea of combining different stress balance approximations has been around for some time, with limited success concerning the inclusion of the Full Stokes equations, so it is great to see a new method being proposed. After the description of the method, several diagnostic and prognostic examples are shown to assess the accuracy of the solution and the gain of the coupling in terms of computational time.

There are several points either unclear or missing in the manuscript that are detailed below, including two critical ones that preclude me from accurately assessing this new method in the current version of this manuscript. The first one is that it is really difficult to follow the derivation of the coupling, because the equations are hard to follow. I understand that this is a very technical problem, but the goal is to describe in a way that is accessible to most interested readers, so some clarifications are needed. The second one is that there is no example showing the impact of the coupling method in a case where the Full Stokes and Shelfy Stream Approximations exhibit a significantly different behavior. This might be the case for the marine ice sheet experiment, but results from the Shelfy Stream Approximations are never shown, so it is impossible to undoubtedly assess the capability of this new coupling method.

Major comments:
The main point of this paper is to describe a new coupling method between the Full Stokes and Shelfy Stream Approximation equations. Unfortunately the current version of the manuscript is written in a way that makes understanding this new method quite challenging. First of all, all the derivation is hidden in the appendix, while it should be the core of the paper. Second, the appendix is a list of equations with no clear path to follow the demonstration, often jumping from one equation to the next with no explanation. Specifically, there should be a few sentences at the beginning explaining the method used to derive the additional force applied at the boundary between the two subdomains. It should be clearly stated when new terms are introduced and where they come from, or if it is a new definition (Let us define X as ...). I tried to understand the derivation of the force, but I must say that I am still quite confused by several parts despite spending ample time on it.

We agree that the manuscript improved when introducing terms and equations more clearly. Specifically, we added information about the additional force, as explained in response to the technical suggestions for p.7 l.8 and l.10, p. 16 and p. 17.
Besides that, we have rewritten the introduction such that it is clearer that the FS-SSA coupling proposed is more a domain decomposition method than actually coupling the stresses themselves. Specific comments are addressed below (suggestions to p. 16-17).

I find the introduction a bit biased to justify the need of this new coupled model. Having the opportunity to combine different stress balance approximations is indeed a genuine idea worth pursuing, and worth some investigations. So there is no need to emphasize the importance of solving a Full Stokes contact problem at the grounding line when

recent studies suggest a limited impact (Pattyn and others, 2013), or to advertise using friction laws that require limited resolution around the grounding line (Gladstone and others, 2013) because it is easier to do with a Full Stokes model that would otherwise require too much computational capabilities to be solved at very high resolution around the grounding line. I would like to see the introduction a bit more in line with the literature, which would not diminish the importance of this manuscript.

Thank you for acknowledging the importance of this manuscript. The interpretation of Pattyn and others (2013) is addressed in the technical suggestion p.2 l.13. The section on a friction law that requires limited resolution around the grounding line (Gladstone and others, 2013) was included because it explains the numerical experiment used in this study. We agree that it was confusing to place this section in the introduction, and may give the impression that we advertise using such a friction law. Therefore, we have moved this part to the description of the numerical experiment where the sliding law in question is applied (Sect. 4.2.1), which will also avoid other confusion with respect to the sliding law (technical suggestion p.21).

The manuscript details the coupling between the Full Stokes and Shelfy Stream Approximations, but there are no details about the other difficulties caused by this coupling. Especially, there is no detail on how the domain is discretized into a 2D and a 3D part, and how this division evolves with time (how is the distance to the grounding line computed? how are elements switched between 2D and 3D?). There is also no detail on how the surface evolution is connected into the two parts of the domain. In one part of the domain, only one equation describing the thickness evolution needs to be solved, while in the other part, two equations describing the evolution of the upper and lower surface elevations need to be solved. Similar to the stress balance equation, some explanations must be added to explain the coupling in the surface evolution equations.
Thank you for pointing out missing information, this will be addressed in technical suggestions p.6 l.1-5, p.7 l.21 and p.14 l.16-18.

The notations in the equations are not always consistent, for example between eq.(4) and eq.(6). They both describe a similar quantity but one is based on the components of the tensor, while the other one is based on the velocity derivatives, for no obvious reasons.
Same for η and $\bar{\eta}$ in eq.(3) and eq.(5). They both depend on the velocity, but in one case the dependence is explicitly stated while it is not in the other case, which tends to be confusing. There are also many terms introduced that are not necessary, adding more confusion.
Thanks for pointing these inconsistencies out. We have made our notations more consistent, by writing eq. (4) (revised manuscript eq. (5)) in velocity derivatives as well. The velocity dependence is removed from eq. (5) and also from Sect. 3.3 where the viscosity was written with velocity dependence.

Results for the marine ice sheet experiment with a pure Shelfy Stream Approximation should be added to see how different the solution is from a Full Stokes model. The objective here is to assess the algorithm in a case where the Shelfy Stream Approximation and Full Stokes solutions are different. We don't know here if this experiment leads to different results with the two stress balance equations, and therefore there is no evidence that the coupling works in a case where the two solutions are different. So until we see how the coupling works in a case where the Shelfy Stream Approximation and Full Stokes equations lead to significantly different solutions, it is not possible to assess the capability of this coupling method to correctly produce an accurate solution

that needs Full Stokes on a part of the domain.

We show the difference between FS and SSA for the marine ice sheet experiment in comment to the technical suggestion p.12. However, we do not agree that a case where the FS and SSA exhibit a significantly different behavior is necessary to assess the capability of the coupling method. On the contrary, coupling the FS and SSA is only feasible in an area where the FS and SSA are alike, otherwise a coupling cannot provide a continuous velocity field. In cases where part of the domain is such that the FS and SSA exhibit a significantly different behavior, the most important task is to find a suitable coupling location, hence where SSA starts to become applicable.

Technical suggestions:
Note that the line numbering on each page starts with a different number, so I did my best to be clear but it might sometimes induce some confusion.
Thank you, we apologize for the confusion in the numbering.

p.1 l.2: “their non-linearlity” → “the non-linearity”
Done.
p.1 l.2: “are used” → “are commonly used”
Done.
p.1 l.8: “periodical temperature” → “periodic temperature”
Done.
p.1 l.10: “modeling an ice sheet complex” → “modeling a complex ice sheet”
We have changed it to ‘*a marine ice sheet*’.
p.1 l.15: increased attention to what? (missing words)
Thank you, we have reformulated the first sentences (see next comment).
p.1 l.16: Quantify “much”. Also it seems that at least in Greenland, the majority of the changes are caused by surface mass balance changes (Enderlin and others, 2014)
Thank you for pointing this out. As mentioned in reply to the first major comment, we have updated our references and stress that the main *uncertainty* comes from dynamic changes.
p.2 l.1: remove “strongly”: some materials rheology are much more non-linear that ice.
Thanks, the equation is strongly non-linear in a mathematical sense, but we agree that it may be confusing to call the rheology strongly non-linear so we have removed “strongly”.
p.2 l.7: add Hindmarsh (2004) as a reference for the hybrid models
Thank you again, this reference is added.
p.2 l.13: I disagree with the interpretation of the Pattyn and others (2013) results. In my opinion they show that models including membrane stress and whose grid resolution is sufficiently small capture grounding line evolution in a relatively similar way.
We have rephrased the interpretation of Pattyn and others (2013), to state that it requires inclusion of vertical shearing and not necessarily Full Stokes and also included one more reference (Pattyn and Durand, 2013) to support this interpretation. Also, we have added a reference to MISMIP+.
“In MISMIP3d, GLD differ between FS models and SSA models, with discrepancies attributed to so-called higher order terms which are neglected in SSA models but included in FS models (Pattyn et al., 2013). Based on these model intercomparisons, it is advised to use models that include vertical shearing to compute reliable projections of ice sheet contribution to sea level rise (Pattyn and Durand, 2013). It should be noted that the experiments in MISMIP3d were idealized, laterally extruded 2D geometries with quite small sideward disturbances and MISMIP+ (Asay-Davis et al., 2016) may give more insight on realistic situations.”

p.2 l.15: “complexes” → “systems”
We have rephrased the sentence, such that this suggestion is not applicable anymore.
p.2 l.17: add a reference for the Ice Sheet System Model
Done, Larour et al. (2012) is added.

p.2 l.23-25: The important question is not so much if friction laws depending on the effective pressure law are faster, but to figure out which ones are more accurate and a allow a good description of the bedrock underlying the ice.
We agreed that the important question is to figure out which sliding law is more accurate. As mentioned in reply to major comment 2, this section was included because it explains the numerical experiment used in this study. To avoid confusion, we have moved this part to the description of the numerical experiment where the sliding law in question is applied (Sect. 4.2.1).
p.3 l.7: "strain rate" → "strain rate tensor"
Done.
p.3 l.15: remove "highly"
Done.
p.3 l.16: I don't see the link between the non-linearity of the Full Stokes model and the derivation of simplified approximations. Most the approximations are also non-linear, and the main purpose of these approximations is to solve a system with less than four coupled unknowns, as is the case with Full Stokes problem.
Agreed, we have reformulated the manuscript,
"Due to the velocity dependence of the viscosity in Eq. (\ref{eq:Glen}), the FS equations are non-linear. Therefore, many approximations to the FS equations have been derived .. "
to
"Due to the velocity dependence of the viscosity in Eq. (\ref{eq:Glen}), the FS equations form a non-linear system with four coupled unknowns, which is time consuming to solve. Therefore, many approximations .."
p.3 l.20: So what terms are neglected in the Shallow Ice Approximation?
We assume that the Shallow Shelve Approximation is meant here. Thanks for pointing this out, we agree that the manuscript benefits from a more detailed description of the SSA and changed:
"For ice shelves, the Shallow Shelf Approximation (SSA), has been derived by dimensional analysis based on a small aspect ratio and surface slope (Morland, 1987; MacAyeal, 1989), such that conservation of linear momentum (Eq. (2)) simplifies to "
to
"For ice shelves, the Shallow Shelf Approximation (SSA), has been derived by dimensional analysis based on a small aspect ratio and surface slope (Morland, 1987; MacAyeal, 1989). This dimensional analysis shows that vertical variation of u and v is negligible, such that w and p can be eliminated by integrating the remaining stresses over the vertical and applying the boundary conditions at the glacier surface and base. Then, the conservation of linear momentum (Eq. (2)) simplifies to"

p.4 l.2: How is p eliminated?
See previous comment.
p.4 l.2: I think the main difference that should be explained is that in the Full Stokes case, one has to solve a 3D problem with 4 unknowns, while in the Shallow Shelf Approximation, one has to solve a 2D problem with 2 unknowns.
Agreed, we clarify this by changing
"The SSA equations are still non-linear through $\bar{\eta}$, but since vertical variation of u and v is neglected, and w and p are eliminated, they are less computationally demanding than FS. " to
"The SSA equations are still non-linear through $\bar{\eta}$, but since w and p are eliminated and vertical variation of u and v is neglected, the 3D problem with 4 unknowns is reduced to a 2D problem with 2 unknowns. Therefore, the SSA model is less computationally demanding than FS."

Fig.1 caption: What is d GL ? Also change "coupling interface" and "grounding line" by "the coupling interface" and "the grounding line"

Thank you for your suggestion, a sentence is added. *"The distance between x_c and x_GL, defined in Eq. (17), is denoted d_GL."*

p.4 l.5: "parametrized" → "represented"
Done.
p.4 Eq.(9): z* does not seem to depend on N in eq.(10).
Thanks for pointing out the confusing notation, the dependence disappears when assuming the hydrostatic balance. We have clarified this by writing "*In line with Gladstone et al. (2017), instead of modeling N, a hydrostatic balance is assumed to approximate z*, .."*
p.5 l.14: "volume gain" is confusing, rephrase.
Rephrased to *"$a_{s/b}$ is the accumulation ($a_{s/b}>0$) or ablation ($a_{s/b}<0$) in meter ice equivalent per year."*
p.5 l.18: Why introduce the ice flux here. This is a new quantity that is never used in the paper, and could be simply replaced by its description (H ū, H v̄)
Agreed, thanks for pointing out this simplification, it is changed in the revised manuscript.
p.5 l.20-23: This 2D/3D explanations are a bit confusing. It is not clear if the SSA part of the model is still in 2D or 3D but the equations are solved only in 1D or 2D on a layer of the model, or if the mesh is indeed changed to 1D or 2D for the SSA, in which case it is not accurate to refer to 2D and 3D models only, and it would be more accurate to say 1D/2D and 2D/3D. Also, there are no details on what is done for the different parts of the mesh.
Thank you for pointing this out, we have rewritten the section such that it is more clear what is meant with 2D and 3D. This section is meant as a theoretical estimate of the memory and performance of a FS-SSA coupling, regardless of the implementation of the coupling, details on what is done for the mesh in the specific coupling presented in the manuscript will be provided in a later section (see comment to p.6 l.1-5 below). We agree that it is not very clear now that we do not consider a specific coupling, and added as a first sentence to this subsection:
"The reduction of the memory required for a FS-SSA coupling by domain decomposition, compared to a FS model, can be estimated. This estimate is independent of the specific implementation of the coupling between the domains."

We have rephrased (see revised manuscript):
"The number of nodes in Ω_FS is then approximately (1 − θ)Nh Nz and in Ω_SSA it is θN_h , neglecting shared nodes on the boundary. For a 3D physical domain, FS and SSA have 4 and 2 unknowns, respectively. Hence, the memory needed to store the solution with a coupled model is proportional to 2Nh (θ + 2(1 − θ)Nz). For a 2D simulation, where FS has 3 unknowns and SSA only 1, the memory is proportional to Nh (θ + 3(1 − θ)Nz)."

p.6 l.1-5: As mentioned just above, we don't have any detail on how the discretization of the problem is done in the two parts, and how they are connected. For example, how is the domain decomposed into 2D and 3D (or 1D and 2D), and how does this evolve with time. Details need to be added to understand this part, especially the connection between the two parts of the domain.

Many thanks for emphasizing this, we have added the following:
"First the velocity $\vec{u}$ (using FS or SSA) is solved for a fixed geometry at time t. The mesh always has the same dimension as the physical modeling domain, but $\vec{u}_{SSA}$ is only solved on the basal layer, after which the solution is reprojected over the vertical axis.
Then, the geometry is adjusted by solving the free surface and thickness advection equations using backward Euler time integration."
Details on the connection between the two parts of the domain are added later, to Section 3.3, see comment to p. 8 l.29.

p.6 l.12: How accurate is the residual free bubbles method?
Different stabilization methods are extensively studied in Gagliardini and Zwinger (2008), and the residual free bubbles method is recommended there, mainly since it provides a better choice on low aspect-ratio elements. This citation is added to the manuscript.

p.7 l.3: “the SSA equations”: maybe add here that they are used as Dirichlet boundary conditions right away, that will be more clear.
Thanks for pointing this out, similarly it is also added that the force boundary condition is of Neumann type. We changed “*The FS velocity at x_c provides an inflow boundary condition to the SSA equations.” to “The FS velocity at x_c provides a Dirichlet inflow boundary condition to the SSA equations.”*

p.7 l.6: What are A and b? Define them.
In other articles, such as Gagliardini et al. (2013), it seems sufficient to define A as the FE system matrix. We have rephrased such that it is more clear that ‘system matrix’ is a definition in FEM terminology.
“*The SSA equations are linearized, and by means of FEM discretized. This leads to a matrix representation Au = b, where u is the vector of unknown variables (here horizontal SSA velocities). In FEM terminology, the vector b that describes the forces driving or resisting ice flow is usually called the body force and A the system matrix (Gagliardini et al., 2013).*¨
p.7 l.8: What is A SSA ? Define it.
A_SSA is A without the Dirichlet conditions being set, more detailed explained in the next comment.

p.7 l.8: “without the Dirichlet conditions”: this is really confusing. It is really hard to follow what is going on here, as none of the terms are explained or detailed.
We agree that information on the way the Dirichlet conditions are set in Elmer/Ice may clarify the derivation of the contact force, therefore we have added
“In Elmer/Ice, Dirichlet conditions for a node i are prescribed by setting the i’th row of A to zero, except for the diagonal entry which is set to be unity, and b_i is set to have the desired value.”

p.7 l.10: see Appendix A: the derivation of the force applied at the interface of the Full Stokes and Shelfy Stream parts of the domain is the core of the paper. This explanation of where this force comes from and how it was derived need to be entirely moved to the main manuscript, and not hidden in an Appendix.
We prefer to describe the coupling in words in the main text and use more mathematical notation and derivations in the Appendix. Since Referee 2 did not complain about this, we prefer to keep it as it was.

p.7 l.12: Why not take the depth-averaged velocity? This would be more consistent with the Shallow Shelf Approximation that computes a vertically integrated solution.
Yes, we agree that this would be more consistent. However, since the coupling requires a (very close to) constant velocity over the vertical, this choice will not significantly affect the results, but is much more straightforward to implement.

p.7 l.21: The surface evolution is solved differently for the two parts of the domain, but no detail is provided on how these two parts are connected, how the equations are actually solved (together or one after the other), and what is the impact in terms of continuity of the surface elevations, or feedback between the two parts.

Thanks for pointing out this missing information. To ensure continuity, H_SSA (x_c) = H_FS (x_c)is applied as a boundary condition to the thickness equation. We have added this to the revised manuscript:
"At x_c , H_SSA = H_FS is applied as a boundary condition to the thickness equation. First the surface evolution is solved for Ω_FS , then Ω_SSA follows."

p.8 l.29: How are the free surface equations solved to ensure continuity of the solution between the two parts of the domain?
We have added the same information as mentioned in previous reply to the algorithm:
"Surface evolution by free surface equations (Eq. (14) for Ω_FS
Surface evolution by thickness equation (Eq. (15)) for Ω_SSA , with H_SSA (x_c) = H_FS (x_c)."

p.10 Fig.3: Consider using round up the numbers in the colorbar. Also "where x c " → "with x c "
Thanks, done.

p.11 l.24: What are the basal conditions applied for this set-up?
We have added a reference to section 2.2.1 where the sliding law is presented, and moved the text on mesh resolution and sliding laws that here, from the introduction:
"Gagliardini et al. (2016) showed that resolving grounding line dynamics with a FS model requires very high mesh resolution around the grounding line. However, Gladstone et al. (2017) showed that the friction law assumed in this study (see Sect. 2.2.1) reduces mesh sensitivity of the FS model compared to the Weertman friction law assumed in Gagliardini et al. (2016), allowing the coarse mesh used here."

p.11 l.25: Describe the "SPIN" experiment.
We have added more information about the SPIN experiment (added information in italics).
"First, the experiment 'SPIN' in Gladstone et al. (2017) is performed, starting from a uniform slab of ice (H=300 m), applying the accumulation in Eq. (22) for 40 kyr, such that a steady state is reached."

p.11 l.11 "minimal" → "small/limited"
Here, "minimal" did not refer to 30 km (which would make it replaceable by "small"), but to d_GL, since 30 km is not the exact distance before applying SSA, but it is the minimal distance between x_GL and x_c (upon mesh resolution this becomes 32.6 km in this case). We have changed
"this small difference shows that the minimal distance d GL before applying SSA is sufficient."
to *"this small difference shows that d _GL=30 km is sufficient."*
p.11 l.11: "For the used mesh resolution" → "For this configuration"
Done.
p.11 l.13: "equal for" → "equal to 30 km for"
Done.
p.11 l.15: Add that the temperature is varied for 500 years and then kept constant for the remaining 2500 years. The equation of the temperature and its description look quite contradictory.
Done.
p.12: results for both diagnostic and prognostic marine ice sheet experiments with a pure SSA model should be added for comparison.
Below, the relative difference [%] between FS and SSA is shown, the relative difference in the grounded part is up to 1.8 percent where u_FS is at least 5 m/yr (not surprising, since basal friction is higher there), on the shelf the relative difference does not exceed 1% (compared to below 0.5% for coupled model). However, we do not consider it necessary to add this result to the manuscript, as argued in response to the last major comment.

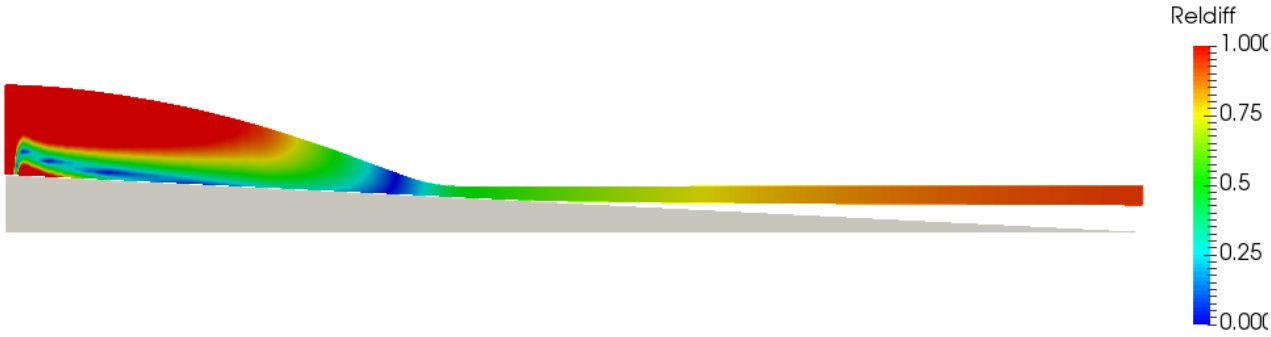

p.13 Fig.6 and Fig.7 captions: “solid line” and “dashed line” → “solid lines” and “dashed lines”
Done.
p.14 l.3: “follows” → “comes”
Done.
p.14 l.16-18: For the prognostic experiment, how is the repartition between the two subdomains computed and set-up? Especially, how is the distance to the grounding line for each point computed (in 3D), and how is the mesh changed from 2D to 3D and vice versa when the grounding line evolves. For elements that are switched from the Shallow Shelf Approximation to the Full Stokes approximation, what is used for the velocity at the beginning of the step, especially the vertical velocity?
The mesh is not changed from 2D to 3D, as addressed in comment p.6 l.1-5. We add information to section 3.3 The algorithm, regarding the setup of the domain decomposition:
“First, the shortest distance d to the grounding line is computed for all nodes in the horizontal footprint mesh at the ice shelf base. Then, a mask is defined that describes whether a node is in Ω_FS , Ω_SSA or at the coupling interface x_c , based on the user defined d_GL. Technically, the domain decomposition is solved by the use of passive elements implemented in the overarching Elmer code (Råback et al., 2016), which allow for deactivating and reactivating of elements. An element in Ω_FS is declared passive for the SSA solver, such that is not included in the global matrix assembly of A_SSA , and vice-versa.”
and regarding switching between domains:
“An element may switch from Ω_SSA to Ω_FS , for example during grounding line advance. Then, the coupled iteration either starts with the initial condition for u_FS if the element is in Ω_FS for the first time, or the latest u_FS (t) computed in this element, before it switched to SSA.”
This holds for both horizontal and vertical velocity. The distance is computed based on the coordinates of the nodes in the basal mesh layer, according to Eq. (16) (Eq. (17) in the revised manuscript), by comparing coordinates and minimizing (called DistanceSolver1, the exact code can be found at
https://github.com/ElmerCSC/elmerfem/blob/d2f371327855ba4b73a0038dcc8ecf4400d25e07/fem/src/modules/DistanceSolve.F90)

p.14 l.5: What is A_FS ? Define it.
Mentioning that it is the system matrix for the FS equations should be enough as definition, as also done in for example Gagliardini et al. (2013).
p.14 l.7: “and and”
Thanks.
p.14 l.19: “the computational work will decrease significantly”. This is quite speculative and should be at least replaced by “is expected to”
Replaced.

p.15 l.11: “multiplying with”: multiplying what?

The entire equation is multiplied by a test function, this is a standard approach to derive the weak formulation on which the FEM is based. We have rephrased:
“After multiplying Eq. (2) with a test function v and integrating over the domain \Omega_FS”.

p.16 l.24: “partly coinciding”: why partly? There is only one interface between the two subdomains.
Yes, there is only one interface, but strictly speaking they only coinciding at the base, where SSA is solved, not entire on the vertical axis. We add information in parentheses:
¨partly coinciding with \Gamma_{FSint} (but of one dimension less)”

p.16 l.11: Eq.(A6) and Eq.(A9) are the same but just rearranged. u_h is not solution of both as it is the same one.
u_h is the finite element approximation of the solution of (A6) and is the solution of (A9) with a particular choice of u_h and v (to be formal).

p.16 l.14: What is f SSA ? Is that how you define it: f SSA = Aṅ? In the case why is the first integral over Γ SSAint and the second one over Γ SSA ? If not, what is f SSA ?
f_{SSA} is defined in Sect 3.1, and now repeated in (A14).
p.17: 20: What about the across flow direction?
Many thanks, we have added information about the lateral boundary condition, denoted as *Γ_l,* to the Appendix, below Eq. (A3):
“Furthermore, there is a lateral boundary Γ_l for Ω_FS ∈ R^3 , where the normal component also vanishes: v|Γ_l ·n = 0 and we assume a vanishing Cauchy-stress vector for unset boundary conditions to velocity components, such that the integral over Γ_l vanishes.”
The same holds for the SSA domain, hence the lateral boundary only affects the definition of the test space in Eq. (A7) and the boundary integral vanishes.

p.17 l.22: I don’t understand where it comes from. You are trying to estimate the last term of Eq.(A4) to apply this force to the Full Stokes part of the domain. The force applied by one subdomain on the other and vice versa are equal, so instead you try to estimate the second term in eq.(A11). But is it ok to have A instead of σ? And how do you get from the weak form to the local equation This sounds pretty abrupt.
There is a force balance on the boundary at Γ_{FSint} and $\Gamma_{SSAint}. The term on the boundary in (A4) is equal to the term on the boundary in (A11) plus the pressure which is eliminated in SSA. Since SSA is integrated in the z-direction, the force has to be scaled by H.
If the integrals in the weak form are equal then the forces in the integrals are equal because they are equal for any v, in particular one with local support. A.n corresponds to the part of \sigma.n depending on the velocity u. The pressure part of \sigma.n corresponds to the cryostatic pressure on the SSA boundary.

p.21: There is no mention in the paper of what friction law is applied.
The friction law is found in Eq. (9) (Eq. (10) in the revised manuscript).

References

Asay-Davis, X. S., Cornford, S. L., Durand, G., Galton-Fenzi, B. K., Gladstone, R. M., Gudmundsson, G. H., Hattermann, T., Holland, D. M., Holland, D., Holland, P. R., Martin, D. F., Mathiot, P., Pattyn, F., and Seroussi, H.: Experimental design for three interrelated marine ice sheet and ocean model intercomparison projects: MISMIP v. 3 (MISMIP+), ISOMIP v. 2 (ISOMIP+) and MISOMIP v. 1 (MISOMIP1), Geosci. Model Dev., 9, 2471–2497, doi:10.5194/gmd-9-2471-2016, 2016.

Gagliardini, O., & Zwinger, T. (2008). The ISMIP-HOM benchmark experiments performed using the Finite-Element code Elmer. *The Cryosphere*, *2*, 67-76.

Gagliardini, O., Zwinger, T., Gillet-Chaulet, F., Durand, G., Favier, L., De Fleurian, B., Greve, R., Malinen, M., Martín, C., and Råback, P.: Capabilities and performance of Elmer/Ice, a new-generation ice sheet model, Geosci. Model Dev., 6, 1299–1318, 2013.

Hindmarsh, R.: A numerical comparison of approximations to the Stokes equations used in ice sheet and glacier modeling, J. Geophys. Res.-Earth, 109, 2004.

Larour, E., Seroussi, H., Morlighem, M., and Rignot, E.: Continental scale, high order, high spatial resolution, ice sheet modeling using the Ice Sheet System Model (ISSM), J. Geophys. Res.-Earth, 117, 2012.

Pattyn, F. and Durand, G.: Why marine ice sheet model predictions may diverge in estimating future sea level rise, Geophys. Res. Lett., 40, 4316–4320, 2013.

Pattyn, F., Perichon, L., Durand, G., Favier, L., Gagliardini, O., Hindmarsh, R. C., Zwinger, T., Albrecht, T., Cornford, S., Docquier, D., et al.: Grounding-line migration in plan-view marine ice-sheet models: Results of the ice2sea MISMIP3d intercomparison, J. Glaciol., 59, 410–422, 2013.

Ritz, C., Edwards, T. L., Durand, G., Payne, A. J., Peyaud, V., and Hindmarsh, R. C.: Potential sea-level rise from Antarctic ice-sheet instability constrained by observations, Nature, 528, 115, 2015.

Anonymous Referee #2 comments and response

We would like to thank the reviewer very much for the time and effort put into reviewing our manuscript. A point-by-point reply (in blue) to each comment (in black) by Referee #2 are given below. Specific changes in the manuscript are written in blue italics.

This work makes modifications to a well-known and widely used glacial flow model Elmer-Ice to allow an approximation to the nonlinear Stokes problem – the Shallow Shelf Approximation – to be solved for a large proportion of the floating part of the domain, in such a way that the two solves are consistent with respect to the force balance. The significance of such a modification is the expense involved with the stokes solve. Not only does it have more degrees of freedom, but it leads to a problem which in the variational sense is a saddle-point and not a minimization problem, leading to difficulty in discretisation; and, though it is not flagged by the authors, there is an extra complication in solving for ice shelves, as a floatation condition cannot be assumed, allowing for oscillation and instability in the vertical momentum condition that must be artificially damped. The work is a nice follow-on slash complement to two other works in the literature: Seroussi et al 2012, which couples together different approximations to the FS problem in a diagnostic setting; and Ahlkrona et al 2016, which dynamically couples FS to SIA in an evolving ice sheet, and is deserving of publication.

We would like to thank you very much for the time and effort you put into reviewing our manuscript.

i only have 2 general comments:

1) My one general comment is that the underlying premise seems to be that this method will reduce computational resource requirements. The reduction in the test cases seems to be low; but this is explained in the discussion, and I am not presently commenting on this. It is rather that presumably this coupling is meant to be applied to regional and continental scale simulations of marine ice sheets. As SSA is only solved on the shelf, the savings are limited by the portion of the domain covered by ice shelves. Quick googling tells me that ice shelves currently represent 10% of Antarctic total area – significantly less than in the test simulations in the paper. So how much more efficient is such a coupling meant to be compared to FS only continental simulations?

When considering the coupling with ISCAL, the gain by having FS-SSA is not just 10% because much of the interior can be modeled with SIA, such that the area left with FS are mainly (around) ice streams and shelves. Also, we are aiming for paleo-simulations, which may have larger ice shelf in the cold period.
We agree that this was not explained in the manuscript yet and have added it to the introduction: *"The extent of present-day ice shelves is limited to approximately 10 % of the area of Antarctica (Rignot et al., 2013). Therefore, one may question the reduction of computational work by applying SSA to model ice shelves in continental scale simulations of marine ice sheets. However, the coupling is targeted to conducting paleo-simulations, for which much larger ice shelves have been present (Jakobsson et al., 2016; Nilsson et al., 2017). Besides that, the new FS-SSA coupling can be combined with ISCAL. Then, a large part of the interior of a marine ice sheet will be modelled with SIA, such that the FS domain will be restricted to ice streams and areas around the grounding line, when SSA is applied to the ice shelves."*

But I am curious about the issue that i bring up in my first paragraph, but was

not addressed. Durand et al 2009 discusses their approach to prevent instability in the vertical due to ice shelves not being in floatation (they added a degree of implicitness to the velocity solver – their eqn 15). I have wondered if this potential instability affects the solution of FS for a marine ice sheet, and possibly artificially enforces archimedean floatation. I would be curious to know about how your coupling affects this issue ,i.e. the need for the "fix" – could you remove the fix for your coupled experiments?

We have not tried to remove the fix for our coupled experiments. In Elmer/Ice, the Stokes and surface evolution equations are coupled by explicit time stepping, because we only solve the coupled system once per each time step. To solve the fully coupled system implicitly is very costly and unnecessary in most of the cases in ice sheet simulation.
One exception is the flotation, since it is a fast process compared to the dynamics of the upper surface of the ice. As you mention, the term added in Durand et al 2009 indeed behaves as an implicit time stepping for the motion of the lower ice surface in contact with water. In this case, it is not an additional term, but the whole eq (15) is an approximation of the surface equation. One can show that by taking the time step sufficiently small, the error in the position of the lower ice surface is as small as we wish in Elmer/Ice and therefore we have not tried to remove it.

2) There is not much discussion on how the FS and SSA domains are updated dynamically (node reassignment etc). Although you touch on it in the discussion, i would like to see a subsection in the methods section briefly detailing this, even if it makes use of already-existing frameworks. Apologies if such text is there and i overlooked it.

Thanks for pointing this out, indeed the manuscript will improve by adding more information on the technical implementation of the coupling, this information is added to Sect. 3.3 The algorithm:
"First, the shortest distance d to the grounding line is computed for all nodes in the horizontal footprint mesh at the ice shelf base. Then, a mask is defined that describes whether a node is in Ω_FS , Ω_SSA or at the coupling interface x_c , based on the user defined d_GL . Technically, the domain decomposition is solved by the use of passive elements implemented in the overarching Elmer code (Råback et al., 2016), which allow for deactivating and reactivating of elements.
An element in Ω_FS is declared passive for the SSA solver, such that is not included in the global matrix assembly of A_SSA , and vice-versa.
An element may switch from Ω_SSA to Ω_FS , for example during grounding line advance. Then, the coupled iteration either starts with the initial condition for u_FS if the element is in Ω_FS for the first time, or the latest u_FS (t) computed in this element, before it switched to SSA."

p2 l 10: MISMIP3D
It is called MISMIP3d in the title of the paper (Pattyn et al., 2013).

p3 line 7: strain rate tensor
Changed.

p3 l 9: here they are just the Stokes equations. ("Full Stokes" arose because glaciologists realised the equations they had been solving for years were an approximation to Stokes with power-law rheology)
Since our main target public are glaciologists we will keep it like that.

eq 4: your notation for the the 2nd invariant of tensors (in this case D) is a bit subtle, you might consider something else – this is simply a suggestion though
We have written out the 2nd invariant in velocity gradients, Eq. (5) in the revised manuscript.

p3 l 22: "h represents the horizontal components" is a bit ambiguous, and you do not

use the subscript in eq (6)
We have rewritten '*h represents the components in the x-y plane*', and have added the subscript to Eq. (6) (Eq. (7) in the revised manuscript) as well.

eq (9): is z* a function of effective pressure, which is not defined, or of H as it appears to explicitly be from eq (10)?
Indeed, it is a function of H, which we clarified by writing
"In line with Gladstone et al. (2017), instead of modeling N, a hydrostatic balance is assumed to approximate z, the dependence on H is written, z*(H)."*

Section 2.3, abbreviations of two dimensions and three dimensions seem awkward, and be clear by 2D you mean the x-z plane.
Thanks for pointing this out, we have rewritten the section concerning two and three dimensions to:
"The number of nodes in Ω F S is then approximately (1 − θ)N h N z and in Ω SSA it is θN h , neglecting shared nodes on the boundary. For a 3D physical domain, FS and SSA have 4 and 2 unknowns, respectively. Hence, the memory needed to store the solution with a coupled model is proportional to 2N h (θ + 2(1 − θ)N z). For a 2D simulation in the x-z plane, where FS has 3 unknowns and SSA only 1, the memory is proportional to N h (θ + 3(1 − θ)N z)."

p 5 l 22: say what 3 variables are for FS in 2D.
After rewriting of the section, this suggestion did not seem applicable anymore.

p 5 l 23: say what you mean by stokes being a saddle-point problem as many readers will not know what this means.
We think this it is not necessary to define a saddle-point problem here, but have rephrased:
"Furthermore, the FS equations are particularly difficult to solve. In mathematical terminology, they pose a saddle-point problem."
p 5 l 23: "with all its consequences for numerical treatment" – give examples of these consequences, with references. Most readers will not be familiar with this literature, and others (like me) will be only familiar with some of it.
We have added *"This requires special numerical treatment such as stabilization of the finite element discretization (e.g., Helanow and Ahlkrona, 2018) and special iterative solvers for the resulting system of linear equations (Benzi et al., 2005). By elimination of the pressure, the SSA equations do not form a saddle-point problem."*

p 6 l 25: just \theta, not \theta Nz
Thanks, changed.

p6 l 26: say this is approximate, as it must be due to boundaries etc.
We have added that it is approximate since boundaries are neglected.

p6 l 6: by "number of unknown variables" do you mean degrees of freedom; or (u,v,w,p) i.e. 4 versus (u,v) i.e. 2? You are saying that, per node, the former takes twice as long to assemble in a matrix versus the latter? I find this difficult to believe in general. What about differing orders of polynomial in the basis functions, and complexity of interaction between DoFs of different variables?
This is also an approximate expression. If the order of the methods is the same and the complexity of the interaction between the components is similar then the formula is an estimate. Changed to:
"The work to assemble the matrices grows linearly with the number of unknown variables. Suppose that this work for FS in 3D is $4C_{FS}N_hN_z$ in the whole domain, for FS $4C_{FS}(1-\theta)N_hN_z$ in Ω_{FS}, and for SSA $2C_{SSA}\theta N_h$ in Ω_{SSA}. The coefficients C_{FS} and C_{SSA} depend on the basis functions for FS and SSA and the

complexity of the equations. The reduction in assembly time for the matrix is $q_{ass}=1-\theta+C_{SSA}\theta/2C_{FS}N_z$. If $C_{FS}\approx C_{SSA}$ then the reduction is approximately as in (16). The same conclusion holds in 2D. Therefore, the reduction of that part is estimated to be similar to the reduction in Eq (15).”

p 6 l 16: is there a theoretical basis for d_{GL} – such as the estimate of the non-hydrostatic boundary layer from Schoof (2011, JFM)? Or arbitrary?
We have no theoretical basis for d_{GL}. As mentioned in the discussion we propose that further studies let Ω SSA be determined automatically, not necessarily based on d_{GL} but for example based on a tolerance for the vertical variation of the horizontal velocities (that should be close to zero in order to allow for a smooth coupling to SSA) or by using a posteriori error estimates based on the residual as derived in Jouvet (2016).
p 7 eq (17): this is an initial guess for the membrane stress at the interface, yes? Would a better one not be \sigma_{FS} \cdot \vec{n} = \rho_w g (-z) if z<0, i.e. the condition which would be applied if xc was a calving front? (This would be exact in the 2D case with no buttressing seaward of x_c; and i wonder if it would reduce iteration count in general)
Good point, probably it would reduce iterations, we have considered this initial guess during the implementation as well. However, this would only be beneficial during the first time step, or when the coupling interface x_c has changed position. Any other time, the algorithm will take f_SSA from the previous iteration and this will thus be a good initial guess.

p 9 l 12: "assembly time ... almost doubles" – i think this is the issue you address in the discussion? would be good to say that it is addressed in the discussion, as i was confused by this when i read it.
Thanks for pointing this out, we have added *“This issue is due to usage of passive elements and is addressed in the Discussion (Sect. 5).”*
p 9 l 15: is v velocity in the y-direction? better say so. aside from no normal flow, what is the other BC at the lateral boundary? no stress? no flow?
We have changed $v=0$ to $u\cdot n=0$. The unset boundary conditions for remaining velocity components, by the natural boundary condition resulting from a partial integration of the stress divergence in the weak formulation, automatically apply a vanishing Cauchy-stress vector in that direction. This information has been added to the Appendix, below Eq. (A3):
“Furthermore, there is a lateral boundary Γ_l for Ω_FS ∈ R^3 , where the normal component also vanishes: v|Γ_l ·n = 0 and we assume a vanishing Cauchy-stress vector for unset boundary conditions to velocity components, such that the integral over Γ_l vanishes.”

p 11 line 8: 58% of the nodes – you mean in the projection of the grid to the x-y plane?
Yes, thanks for pointing this out, changed to “58% of the nodes in the horizontal footprint mesh are located inside \Omega_{SSA} (θ = 0.58)”.
p 12 paragraph at line 13: found this discussion a bit difficult to follow – is there any way the main performance points can be summarised in a table? also limited –> varied
Thanks for pointing this out, we have added a table and reduced the amount of information in this paragraph, referring to the table instead.

p 14 discussion at line 10: if you were to make this change re: node assignment at a lower level, how would it affect the ability to easily update the Full Stokes sub-domain?
This would not affect the ability to easily update the Full Stokes sub-domain, it would be based on the same mask as the passive/active updates are done now (see the extra information added in Sect. 3.3, in reply to the second general comment). It was shown for ISCAL that this can be done efficient and dynamically in Elmer/Ice (Ahlkrona et al. 2016).

p 16 line 24: you previously used A as a symbol for a matrix
Thanks, changed to B such that there is no confusion with A being previously defined as a system matrix. However, B (or A in old version) is a matrix, with derivatives in the elements.
p 16 line 4: did you define f_{CF}?
We had only given the FS version of the boundary condition at the calving front (Eq. (12), (13) in the revised manuscript) and added: *"f_{CF}, as in Eq. (13) but integrated over z"* to the Appendix.
p 16 eq (A7) and below: suggest to use w as a test function symbol
We chose to stick to v for a test function.
p 16 eq (A9) the 1st boundary integral is over \Gamma_{SSA} not \Gamma_{SSAint}
Indeed, updated.

References

Ahlkrona, J., Lötstedt, P., Kirchner, N., & Zwinger, T. (2016). Dynamically coupling the non-linear Stokes equations with the Shallow Ice Approximation in glaciology: Description and first applications of the ISCAL method. *Journal of Computational Physics*, *308*, 1-19.

Benzi, M., Golub, G. H., and Liesen, J.: Numerical solution of saddle point problems, Acta Numer., 14, 1–137, 2005.

Helanow, C. and Ahlkrona, J.: Stabilized equal low-order finite elements in ice sheet modeling–accuracy and robustness, Computat. Geosci.,
pp. 1–24, 2018.

Jakobsson, M., Nilsson, J., Anderson, L., Backman, J., Björk, G., Cronin, T. M., Kirchner, N., Koshurnikov, A., Mayer, L., Noormets, R.,
et al.: Evidence for an ice shelf covering the central Arctic Ocean during the penultimate glaciation, Nat. Commun., 7, 10 365, 2016.

Jouvet, G.: Mechanical error estimators for shallow ice flow models, J. Fluid Mech., 807, 40–61, 2016

Nilsson, J., Jakobsson, M., Borstad, C., Kirchner, N., Björk, G., Pierrehumbert, R. T., and Stranne, C.: Ice-shelf damming in the glacial Arctic Ocean: dynamical regimes of a basin-covering kilometre-thick ice shelf, The Cryosphere, 11, 1745, 2017.

Pattyn, F., Perichon, L., Durand, G., Favier, L., Gagliardini, O., Hindmarsh, R. C., Zwinger, T., Albrecht, T., Cornford, S., Docquier, D., et al.: Grounding-line migration in plan-view marine ice-sheet models: Results of the ice2sea MISMIP3d intercomparison, J. Glaciol., 59, 410–422, 2013.

Dynamically coupling Full Stokes and Shallow Shelf Approximation for marine ice sheet flow using Elmer/Ice (v8.3)

Eef C. H. van Dongen[1,2,3,4], Nina Kirchner[2,5], Martin B. van Gijzen[3], Roderik S. W. van de Wal[4], Thomas Zwinger[6], Gong Cheng[5,7], Per Lötstedt[5,7], and Lina von Sydow[5,7]

[1]Laboratory of Hydraulics, Hydrology and Glaciology, ETHZ, Zurich, Switzerland
[2]Department of Physical Geography, Stockholm University, Stockholm, Sweden
[3]Department of Applied Mathematical Analysis, Delft University of Technology, Delft, The Netherlands
[4]Institute for Marine and Atmospheric Research Utrecht, Utrecht University, The Netherlands
[5]Bolin Centre for Climate Research, Stockholm University, Stockholm, Sweden
[6]CSC-IT Center for Science, Espoo, Finland
[7]Division of Scientific Computing, Department of Information Technology, Uppsala University, Uppsala, Sweden

Correspondence to: E. C. H. van Dongen (vandongen@vaw.baug.ethz.ch)

Abstract. Ice flow forced by gravity is governed by the Full Stokes (FS) equations, which are computationally expensive to solve due to ~~their~~ the non-linearity introduced by the rheology. Therefore, approximations to the FS equations are commonly used, especially when modelling ~~an ice sheet complex~~ a marine ice sheet (ice sheet, ice shelf and/or ice stream) ~~on the order of~~ for 10^3 years or longer. The Shallow Ice Approximation (SIA) and Shallow Shelf Approximation (SSA) are commonly used but are accurate only ~~in~~ for certain parts of an ice sheet. Here, we report ~~on~~ a novel way of iteratively coupling FS and SSA that has been implemented in Elmer/Ice and applied to conceptual marine ice sheets. The FS-SSA coupling appears to be very accurate; the relative error in velocity compared to FS is below 0.5% for diagnostic runs and below 5% for prognostic runs. Results for grounding line dynamics obtained with the FS-SSA coupling are similar to ~~results~~ those obtained from a FS model in an experiment with a periodical temperature forcing over 3000 years ~~inducing~~ that induces grounding line advance and retreat. The rapid convergence of the FS-SSA coupling shows a large potential in reducing computation time, such that modelling ~~an ice sheet complex~~ a marine ice sheet for thousands of years should become feasible in the near future. Despite inefficient matrix assembly in the current implementation, computation time is reduced ~~significantly, i.e.~~ by 32%, when the coupling is applied to a 3D ice shelf. ~~In the future, the FS-SSA coupling can be extended to include a SIA-FS coupling of ISCAL (Ice Sheet Coupled Approximation Level)-type.~~

1 Introduction

~~Observations of contemporary mass loss from ice sheets have attracted increased attention due to the importance of sea level changes for society (Church et al., 2013). Much of this mass loss is the result of ice dynamics, rather than due to elevated temperatures causing increased surface melt (Schoof and Hewitt, 2013).~~ Dynamical changes in both the Greenland and Antarctic ice sheets are, with medium confidence, projected to contribute 0.03 to 0.20 m of sea level rise by 2081-2100 ~~,~~ ~~but a limited understanding of ice dynamics is the~~ (Church et al., 2013). The main reason for the uncertainty in these estimates

(Church et al., 2013)is a limited understanding of ice dynamics. Thus, there is a great need for improvement of ice dynamical models . The gravity driven (Ritz et al., 2015). The gravity-driven flow of ice is described by the Full Stokes (FS) equations, amended by a strongly non-linear rheology described by Glen's flow law. Model validation is required over centennial to millennial time scales in order to capture the long response time of an ice sheet to external forcing (Alley et al., 2005; Phillips et al., 2010; Stokes et al., 2015). However, the computation time and memory required for a FS model to be applied to ice sheets restricts simulations to sub-millenial timescales (Gillet-Chaulet et al., 2012; Gladstone et al., 2012a; Nowicki et al., 2013; Seddik et al., 2012; Joughin et al., 2014; Seddik et al., 2017). Therefore, approximations of the FS equations are employed for simulations over long timescales, such as the Shallow Ice Approximation (SIA, Hutter, 1983), the Shallow Shelf Approximation (SSA, Morland, 1987; MacAyeal, 1989), Blatter-Pattyn (Pattyn, 2003)or hybrid models (Bernales et al., 2017) are employed for simulations over long timescales, and hybrid models (Hindmarsh, 2004; Bernales et al., 2017).

Any ice sheet model accounting for ice shelves needs to resolve grounding line dynamics (GLD). Despite many recent efforts, modelling GLD still poses a challenge in numerical models, as illustrated by the wide range of results obtained in the Marine Ice Sheet Model Intercomparison Project (MISMIP). In MISMIP(MISMIP, Pattyn et al., 2012). In MISMIP3d, GLD differ considerably between FS models and non-FS SSA models, with discrepancies attributed to so-called higher order terms which are neglected in SSA models but included in FS models (Pattyn et al., 2012). Consequently, there appears to emerge a consensus that accurate simulation of GLD requires solving the FS equations near the grounding line (Pattyn et al., 2013) (Pattyn et al., 2013). Based on these model intercomparisons, it is advised to use models that include vertical shearing to compute reliable projections of ice sheet contribution to sea level rise (Pattyn and Durand, 2013). It should be noted that the experiments in MISMIP3d were idealized, laterally extruded 2D geometries with quite small sideward disturbances and MISMIP+ (Asay-Davis et al., 2016) may give more insight on realistic situations.

Since solving Solving the FS equations over large spatio-temporal domains is still infeasible. However, solvers combining approximations (e.g. SIA or SSA) with the FS equations allow to simulate the dynamics of ice sheet complexes simulation of ice dynamics over long time spans without introducing artifacts caused by application of approximations in parts of the domain where they are not valid. For instance, Seroussi et al. (2012) coupled FS and SSA, in the framework of the Ice Sheet System Model (ISSM), applying (ISSM, Larour et al., 2012). They apply the Tiling method which includes a blending zone of FS and SSA. Their result looks promising with respect to both accuracy and efficiency, but is limited to diagnostic experimentsonly. Here, we present a novel coupling between FS and SSA . The Ice Sheet Coupled Approximation Levels (ISCAL) method (Ahlkrona et al., 2016) couples SIA and FS by a non-overlapping domain decomposition that dynamically changes with time. ISCAL is implemented in Elmer/Ice (Gagliardini et al., 2013), an open source finite element software for ice sheet modelling, by . Here, we present a novel coupling between FS and SSA, also by implementation of a non-overlapping domain decomposition that changes with timein Elmer/Ice. The domain decomposition changes dynamically with grounding line advance and retreat. GLD are modelled with FS , and coupled to SSA on the ice shelf via boundary conditions. The equations discretized by the finite element method are solved iteratively, alternating between the FS and the SSA domain, until convergence is reached.

The extent of present-day ice shelves is limited to approximately 10 % of the area of Antarctica (Rignot et al., 2013). Therefore, one may question the reduction of computational work by applying SSA to model ice shelves in continental scale simulations of marine ice sheets. ~~Gagliardini et al. (2016) showed that resolving GLD with a FS model requires very high mesh resolution around the grounding line, which explains why recent studies on GLD applied the SSA instead (e.g., Brondex et al., 2017) .~~ However, ~~Gladstone et al. (2017) showed that the effective pressure-dependent friction law assumed in this study (see Sect. 2.2.1) reduces mesh sensitivity of the FS model compared to~~ the ~~Weertman friction law assumed in Gagliardini et al. (2016), allowing for a coarser mesh~~coupling is targeted to conducting paleo-simulations, for which much larger ice shelves have been present (Jakobsson et al., 2016; Nilsson et al., 2017). In that case, a large part of the interior of a marine ice sheet is modelled with SIA, SSA is applied to the ice shelves and the FS domain is restricted to ice streams and areas around the grounding line.

An overview of the FS and SSA equations governing ice sheet and shelf dynamics in three dimensions (3D) is presented in Sect. 2, together with the boundary conditions~~and memory and~~ . Memory and performance estimates of ~~the~~ a FS-SSA coupling~~. In Sect. 3,~~ , independent of the specific coupling implemented, are provided in Sect. 2.3. Section 3 describes the coupled FS-SSA model~~(hereafter '*coupled model*') is described~~, hereafter 'coupled model'. The coupling is applied to a conceptual ice shelf ramp and marine ice sheet in Sect. 4. The simulation of a 3000 years long cycle of grounding line advance and retreat (described in Sect. 4.2.2) shows the robustness of the coupling. ~~Results of the experiments are discussed in Sect. 5 and implications for further developments in the coupling of approximation levels are discussed in Sect. ??.~~

2 Governing equations of ice flow

Ice is considered as an incompressible fluid, such that mass conservation implies that the velocity is divergence-free,

$$\nabla \cdot \boldsymbol{u} = 0, \tag{1}$$

where $\boldsymbol{u} = (u, v, w)^T$ describes the velocity field of the ice with respect to a Cartesian coordinate system $(x, y, z)^T$ where z is the vertical direction. For ice flow, the acceleration term can be neglected in the Navier-Stokes equations (Hutter, 1982). Therefore, the conservation of linear momentum under the action of gravity $\boldsymbol{g}$ can be described by

$$-\nabla p + \nabla \cdot \left(\eta \left(\nabla \boldsymbol{u} + (\nabla \boldsymbol{u})^T \right) \right) + \rho \boldsymbol{g} = \boldsymbol{0}, \tag{2}$$

where ∇ is the gradient operator, p pressure, η viscosity, ρ ice density and $\boldsymbol{g}$ denotes gravity. Letting $\boldsymbol{\sigma}$ denote the stress tensor, pressure p is the mean normal stress ($p = -1/3 \Sigma_i \sigma_{ii}$), and $\mathbf{D}(\boldsymbol{u})$ is the strain rate tensor, related by

$$\boldsymbol{\sigma} = 2\eta \mathbf{D}(\boldsymbol{u}) - p\mathbf{I} = \eta \left(\nabla \boldsymbol{u} + (\nabla \boldsymbol{u})^T \right) - p\mathbf{I}, \tag{3}$$

where $\mathbf{I}$ is the identity tensor. Together, Eq. (1) and Eq. (2) are called the Full Stokes (FS) equations. Observations by Glen (1952) suggest that the viscosity depends on temperature T and the effective strain rate $D(\boldsymbol{u})$,

$$\eta(\boldsymbol{u}, T) = \frac{1}{2} \mathcal{A}(T)^{-1/n} D(\boldsymbol{u})^{(1-n)/n}, \; D(\boldsymbol{u}) = \sqrt{\frac{1}{2} \left(D_{xx}^2 + D_{yy}^2 + D_{zz}^2 \right) + D_{xy}^2 + D_{xz}^2 + D_{yz}^2},$$

$$\eta(\boldsymbol{u},T) = \frac{1}{2}\mathcal{A}(T)^{-\frac{1}{n}} D(\boldsymbol{u})^{\frac{1-n}{n}}, \tag{4}$$

$$D(\boldsymbol{u}) = \sqrt{\frac{1}{2}\left(\left(\frac{\partial u}{\partial x}\right)^2 + \left(\frac{\partial v}{\partial y}\right)^2 + \left(\frac{\partial w}{\partial z}\right)^2\right) + \frac{1}{4}\left(\left(\frac{\partial u}{\partial y} + \frac{\partial v}{\partial x}\right)^2 + \left(\frac{\partial u}{\partial z} + \frac{\partial w}{\partial x}\right)^2 + \left(\frac{\partial v}{\partial z} + \frac{\partial w}{\partial y}\right)^2\right)}, \tag{5}$$

where Glen's exponent $n = 3$~~is assumed and D_{ij} are components of $\mathbf{D}(\boldsymbol{u})$~~. The fluidity parameter $\mathcal{A}$ increases exponentially with temperature as described by the Arrhenius relation (Paterson, 1994). This represents a thermodynamically coupled system of equations. However, in the current study, we focus on the mechanical effects and a uniform temperature is assumed. Due to the velocity dependence of the viscosity in Eq. (4), the FS equations ~~are highly~~ form a non-linear system with four coupled unknowns, which is time consuming to solve. Therefore, many approximations to the FS equations have been derived in order to model ice sheet dynamics on long timescales, see Sect. 2.1.

2.1 Shallow Shelf Approximation

Floating ice does not experience basal drag, hence all resistance comes from longitudinal stresses or lateral drag at the margins. For ice shelves, the Shallow Shelf Approximation (SSA), has been derived by dimensional analysis based on a small aspect ratio and surface slope (Morland, 1987; MacAyeal, 1989). This dimensional analysis shows that vertical variation of u and v is negligible, such that w and p can be eliminated by integrating the remaining stresses over the vertical and applying the boundary conditions at the glacier surface and base (described in Sect. 2.2). Then, the conservation of linear momentum~~(~~, Eq. (2)~~) simplifies to~~ , simplifies to

$$\nabla_h \cdot \left(2\bar{\eta}()(\mathbf{D_h}(\boldsymbol{u}) + \mathrm{tr}(\mathbf{D_h}(\boldsymbol{u}))\mathbf{I})\right) = \rho g H \nabla_h z_s \tag{6}$$

where the subscript h represents the ~~horizontal components~~ components in the $x-y$ plane, $\bar{\eta}$ the vertically integrated viscosity, H the thickness of the ice shelf and z_s the upper ice surface, see Fig. 1. The effective strain rate in Eq. (~~4~~5) simplifies to

$$D_{\underline{h}}(\boldsymbol{u}) = \sqrt{\left(\frac{\partial u}{\partial x}\right)^2 + \left(\frac{\partial v}{\partial y}\right)^2 + \frac{\partial u}{\partial x}\frac{\partial v}{\partial y} + \frac{1}{2}\left(\frac{\partial u}{\partial y} + \frac{\partial v}{\partial x}\right)^2}\sqrt{\left(\frac{\partial u}{\partial x}\right)^2 + \left(\frac{\partial v}{\partial y}\right)^2 + \frac{\partial u}{\partial x}\frac{\partial v}{\partial y} + \frac{1}{4}\left(\frac{\partial u}{\partial y} + \frac{\partial v}{\partial x}\right)^2}, \tag{7}$$

where w is eliminated using incompressibility~~(~~, Eq. (1)~~)~~. The SSA equations are still non-linear through $\bar{\eta}$, but since w and p are eliminated and vertical variation of u and v is neglected, ~~and w and p are eliminated, they are~~ the 3D problem with 4 unknowns is reduced to a 2D problem with 2 unknowns. Therefore, the SSA model is less computationally demanding than FS. The horizontal velocities are often of main interest, for example when results are validated by comparison to observed horizontal surface velocity. If desirable, the vertical velocity can be computed from the incompressibility condition~~(Eq. (1)).~~ .

2.2 Boundary conditions and time evolution

The coupling is applied to a marine ice sheet, with bedrock lying (partly) below sea level (see Fig. 1), and involves boundaries in contact with the bedrock, ocean and atmosphere. The only time dependency is in the evolution of the free surfaces.

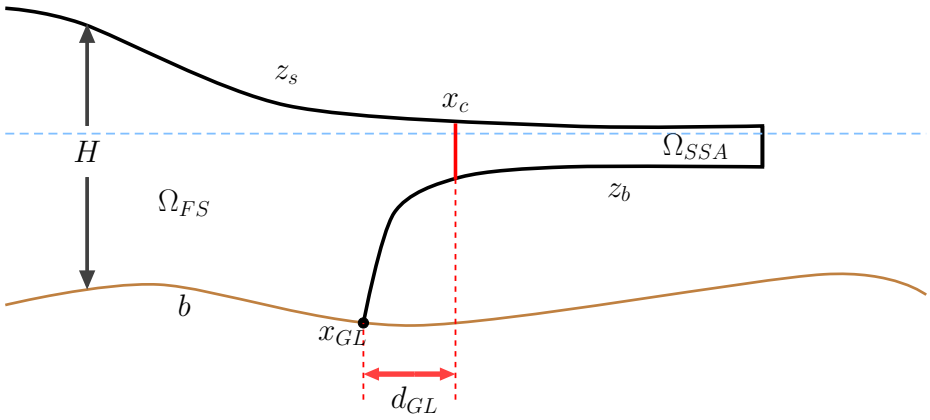

Figure 1. Overview of the notations and domain decomposition for a conceptual marine ice sheet~~with ice shelf~~. The vertical scale is exaggerated. The sea level at $z = 0$ is dashed blue and the interface between the FS and SSA domains is solid red. The bed elevation is denoted by b, the coupling interface by x_c and the grounding line by x_{GL}. The distance between x_c and x_{GL}, defined in Eq. (17), is denoted d_{GL}.

2.2.1 Bedrock

Where the ice is grounded (in contact with the bedrock), the interaction of ice with the bedrock is commonly ~~parametrized~~ represented by a sliding law $f(\boldsymbol{u}, N)$, that relates the basal velocity $\boldsymbol{u}_b$ and effective pressure N to the basal shear stress as

$$(\boldsymbol{t}_i \cdot \boldsymbol{\sigma} \cdot \boldsymbol{n})_b = f(\boldsymbol{u}, N)\boldsymbol{u} \cdot \boldsymbol{t}_i, \ i = 1, 2, \tag{8}$$

$$(\boldsymbol{u} \cdot \boldsymbol{n})_b + a_b = 0, \tag{9}$$

where $\boldsymbol{t}_i$ are the vectors spanning the tangential plane, $\boldsymbol{n}$ is the normal to the bed, and a_b describes basal refreezing or melt. A sliding law suggested by Budd et al. (1979) is assumed~~here~~ , which depends on $\boldsymbol{u}_b$ and the height above buoyancy z_* such that

$$f(\boldsymbol{u}, N) = -\beta |\boldsymbol{u}_b|^{\frac{1}{n}-1} z_*(N). \tag{10}$$

Here, the sliding parameter β is ~~assumed to be~~ constant in time and space. In line with Gladstone et al. (2017), ~~z_* is approximated by~~ instead of modeling N, a hydrostatic balance ~~(~~is assumed to approximate z_*, implying a sub-glacial hydrology system entirely in contact with the ocean~~) as~~ ,

$$z_*(H) = \begin{cases} H & \text{if } z_b \geq 0, \\ H + z_b \frac{\rho_w}{\rho} & \text{if } z_b < 0, \end{cases} \tag{11}$$

where z_b is the lower ice surface, ρ_w the water density and the sea level is at $z = 0$. Equation (11) implies that z_* equals zero ~~as soon as~~ when the flotation criterion (Archimedes' principle) is satisfied, i.e. where

$$z_s = \left(1 - \frac{\rho}{\rho_w}\right) H, \ z_b = -\frac{\rho}{\rho_w} H. \tag{12}$$

2.2.2 Ice-ocean interface

As soon as the seawater pressure p_w at the ice base z_b is larger than the normal stress exerted by the ice at the bed, the ice is assumed to float. For a detailed description of the implementation of the contact problem at the grounding line in Elmer/Ice, see Durand et al. (2009). At the ice-ocean interface, the tangential friction is neglected ($f(\boldsymbol{u}, N) \equiv 0$ in Eq. (8)) and

$$\boldsymbol{\sigma} \cdot \boldsymbol{n} = -p_w \boldsymbol{n} \text{ where } p_w(z) = -\rho_w g z \text{ if } z \leq 0, \tag{13}$$

and $\boldsymbol{\sigma} \cdot \boldsymbol{n} = 0$ above sea level ($z > 0$). Calving at the seaward front of the ice shelf is not explicitly modelled but the length of the modelling domain is fixed and ice flow from the shelf out of the domain is interpreted as a calving rate.

2.2.3 Surface evolution

Ice surface (assumed stress-free, $\boldsymbol{\sigma} \cdot \boldsymbol{n} = 0$) and ice base at z_s and z_b behave as free surfaces according to

$$\frac{\partial z_{s/b}}{\partial t} + u_{s/b}\frac{\partial z_{s/b}}{\partial x} + v_{s/b}\frac{\partial z_{s/b}}{\partial y} = w_{s/b} + a_{s/b}, \tag{14}$$

where $a_{s/b}$ is the ~~rate of volume gain ($a_{s/b} > 0$, accumulation) or loss~~ accumulation ($a_{s/b} > 0$) or ablation ($a_{s/b} < 0$~~, ablation) per unit area~~) in meter ice equivalent per year, at the surface or base, respectively. By vertical integration of the incompressibility condition~~(~~, Eq. (1)~~)~~, w can be eliminated using Leibniz integration rule and substituting the free surface equations~~(~~, Eq. (14), which yields the thickness advection equation

$$\frac{\partial H}{\partial t} + \frac{\partial q_x}{\partial x}\frac{\partial H\bar{u}}{\partial x} + \frac{\partial q_y}{\partial y}\frac{\partial H\bar{v}}{\partial y} = a_s - a_b, \tag{15}$$

where ~~$\boldsymbol{q} = (q_x, q_y)$ is~~ $\bar{u}, \bar{v}$ are the vertically integrated horizontal ~~velocity, also called ice flux~~velocities.

2.3 Memory and performance estimates of a FS-SSA coupling

The reduction of the memory required for a FS-SSA coupling by domain decomposition, compared to a FS model, can be estimated. This estimate is independent of the specific implementation of the coupling between the domains. The main advantage of the SSA model is that $\boldsymbol{u}_{SSA}$ is independent of z, such that the SSA equations can be solved on a part of the domain with a mesh of one dimension fewer. ~~There are also fewer unknowns ; in 3D there are only two unknowns (u and v) compared to four in FS (u, v, w, and p) , and in 2D there is only one compared to FS's three. Besides that, by elimination of the pressure, the~~ Besides that, there are fewer unknowns since p and w are eliminated. An additional advantage of eliminating p is that the resulting system is mathematically easier to discretise and solve. In particular, difficulties related to a stable choice for the basis functions for the pressures and velocities are avoided (see e.g., Helanow and Ahlkrona, 2018)) and there is no need for specialised iterative solution techniques to solve the so-called saddle-point problem ~~imposed by FS (with all its consequences for numerical treatment) can be avoided in SSA~~that the FS equations pose (see Benzi et al., 2005).

Suppose that the computational domain Ω is discretized with N_z nodes regularly placed in the z direction, N_h nodes in a horizontal footprint mesh and decomposed in two parts (Ω_{SSA} and Ω_{FS}, see Fig. 1). The fraction of nodes in Ω_{SSA} is ~~θN_h~~

denoted θ with $0 < \theta < 1$. The number of nodes in ~~3D in~~ Ω_{FS} is then approximately $(1-\theta)N_h N_z$ and in Ω_{SSA} it is θN_h~~.~~, neglecting shared nodes on the boundary. For a 3D physical domain, SSA has 2 unknowns (u and v) and FS has 4 unknowns (u, v, w, and p). Hence, the memory needed to store the solution with a coupled model is proportional to $2N_h(\theta+2(1-\theta)N_z)$~~in 3D and $N_h(\theta+3(1-\theta)N_z)$ in~~. For a 2D simulation in the $x-z$ plane, where FS has 3 unknowns and SSA only 1, the memory is proportional to $N_h(\theta+3(1-\theta)N_z)$. The memory requirement for a physical domain in d dimensions, reduces to

$$q_{\text{var}} = \frac{\text{(SSA + FS) memory}}{\text{FS memory}} \frac{\text{coupled model memory}}{\text{FS model memory}} = 1-\theta+\frac{\theta}{(5-d)N_z},\ d=2,3, \tag{16}$$

when part of the domain is modelled by the SSA equations. The memory requirements for mesh related quantities reduces to $q_{\text{mesh}} = 1-\theta+\theta/N_z$ in both 2D and 3D. The quotients q_{var} and q_{mesh} are close to $1-\theta$ if $N_z \gtrsim 10$.

The computational work is more difficult to estimate *a priori* since it depends on the implementation of the coupling. The dominant costs are for the assembly of the finite element matrices, the solution of the nonlinear equations, and an overhead for administration in the solver. The work to assemble the matrices grows linearly with the number of unknown variables. ~~Therefore~~ Suppose that this work for FS in 3D is $4C_{FS}N_hN_z$ in the whole domain, for FS $4C_{FS}(1-\theta)N_hN_z$ in Ω_{FS}, and for SSA $2C_{SSA}\theta N_h$ in Ω_{SSA}. The coefficients C_{FS} and C_{SSA} depend on the basis functions for FS and SSA and the complexity of the equations. The reduction in assembly time for the matrix is $q_{ass} = 1-\theta+C_{SSA}\theta/2C_{FS}N_z$. If $C_{FS} \approx C_{SSA}$ then the reduction is approximately as in Eq. (16). The same conclusion holds in 2D. Therefore, the reduction of that part is ~~expected to be as~~ estimated to be similar to the reduction in Eq. (16).

3 Method for coupling FS and SSA

All equations are solved in Elmer/Ice (Gagliardini et al., 2013) using the Finite Element Method (FEM). First the velocity $\boldsymbol{u}$ (using FS or SSA) is solved for a fixed geometry at time t~~, then the~~. The mesh always has the same dimension as the physical modeling domain, but $\boldsymbol{u}_{SSA}$ is only solved on the basal mesh layer, after which the solution is reprojected over the vertical axis. Then, the geometry is adjusted by solving the free surface and thickness advection equations using backward Euler time integration. The non-linear FS and SSA equations are solved using a Picard iteration. The discretized FS equations ~~form a saddle-point problem and~~ are stabilized by the residual free bubbles method ~~as explained in Baiocchi et al. (1993). First~~(Baiocchi et al., 1993), the recommended stabilization method in Gagliardini and Zwinger (2008). First, the coupling for a given geometry is presented, followed by the coupled surface evolution, both summarized in Algorithm 1.

The FS domain Ω_{FS} contains the grounded ice and a part of the shelf around the grounding line, see Fig. 1. The SSA domain Ω_{SSA} is restricted to a part of the ice shelf and starts at the coupling interface $\boldsymbol{x}_c$ at the first basal mesh nodes located at least a ~~horizontal~~ distance d_{GL} from the grounding line $\boldsymbol{x}_{GL}$, such that

$$||\boldsymbol{x}-\boldsymbol{x}_{GL}||_h := \sqrt{(x-x_{GL})^2+(y-y_{GL})^2}\sqrt{(x-x_{GL})^2+(y-y_{GL})^2+(z-z_{GL})^2} \geq d_{GL} \text{ for all } \boldsymbol{x} \text{ in } \Omega_{SSA}. \tag{17}$$

3.1 Boundary conditions at the coupling interface

Horizontal gradients of the velocity are not neglected in the SSA equations (unlike in the SIA, Hutter, 1983). Thus, not only FS and SSA velocities have to ~~be coupled by matching those stresses~~match but also their gradients, in order to allow a coupling of the two. Therefore, one cannot solve one system of equations ~~first~~independently, for use as an input to the other system, as done for a one-way coupling (e.g., Ahlkrona et al., 2016). Instead, the coupling of FS and SSA is solved iteratively, updating the interaction between FS and SSA velocities in each iteration to obtain mutually consistent results.

SSA governed ice shelf flow is greatly influenced by the inflow velocity from the FS domain~~, therefore~~ . Therefore, we start the first iteration of the coupled model by solving the FS equations. A boundary condition is necessary at $\boldsymbol{x}_c$, we assume that the cryostatic pressure acts on Ω_{FS} at $\boldsymbol{x}_c$,

$$\boldsymbol{\sigma}_{FS} \cdot \boldsymbol{n}(\boldsymbol{x}_c, z) = \rho g (z_s - z)\boldsymbol{n}, \tag{18}$$

where $\boldsymbol{n}$ is normal to the coupling interface $\boldsymbol{x}_c$. The FS velocity at ~~$\boldsymbol{x}_c$ provides an~~ x_c provides a Dirichlet inflow boundary condition to the SSA equations. Then, the ~~force~~ Neumann boundary condition in Eq. (18) has to be adjusted based on the ice flow as calculated for Ω_{SSA}. This is done using the contact force denoted by $\boldsymbol{f}_{SSA}$, as explained below. ~~In the FEM implemented in Elmer/Ice, the SSA equations (Eq. (6)),~~

The SSA equations are linearized, ~~discretized and rewritten in matrix form~~ and by means of FEM discretized. This leads to a matrix representation $\mathbf{A}\boldsymbol{u} = \boldsymbol{b}$, where $\boldsymbol{u}$ is the vector of unknown variables (here horizontal SSA velocities)~~,~~. In FEM terminology, the vector $\boldsymbol{b}$ that describes the forces driving or resisting ice flow ~~,~~is usually called the body force and $\mathbf{A}$ ~~is~~ the system matrix ~~.~~(Gagliardini et al., 2013). In Elmer/Ice, Dirichlet conditions for a node i are prescribed by setting the ith row of $\mathbf{A}$ to zero, except for the diagonal entry which is set to be unity, and $\boldsymbol{b}_i$ is set to have the desired value (Råback et al., 2016) . For an exact solution of $\mathbf{A}\boldsymbol{u} = \boldsymbol{b}$, the residual $\boldsymbol{f} = \mathbf{A}\boldsymbol{u} - \boldsymbol{b}$ is zero. If we instead use the system matrix $\mathbf{A}_{SSA}$ obtained without the Dirichlet conditions being set, the resulting residual is equal to the contact force that would have been necessary to produce the velocity described by the Dirichlet boundary condition. Since the SSA equations are vertically integrated, $\boldsymbol{f}_{SSA} = \mathbf{A}_{SSA}\boldsymbol{u}_{SSA} - \boldsymbol{b}_{SSA}$ is the vertically integrated contact force and needs to be scaled by the ice thickness H. In Elmer/Ice, $\boldsymbol{f}_{SSA}$ is mesh dependent and needs to be scaled by the horizontal mesh resolution ω as well. For 2D configurations, $\omega = 1$. Using $\boldsymbol{f}_{SSA}$ instead of explicitly calculating the stress is advantageous since it is extremely cheap to find the contact force if $\mathbf{A}_{SSA}$ is stored.

To summarize the boundary conditions at $\boldsymbol{x}_c$, for FS, an external pressure is applied,

$$\boldsymbol{\sigma}_{FS} \cdot \boldsymbol{n}(\boldsymbol{x}_c, z) = \rho g (z - z_s)\boldsymbol{n} + \frac{\boldsymbol{f}_{SSA}(\boldsymbol{x}_c)}{\omega H}, \tag{19}$$

where $\boldsymbol{f}_{SSA} := 0$ in the first iteration (for its derivation, see Appendix A). For SSA, a Dirichlet inflow boundary condition

$$\boldsymbol{u}_{SSA}(\boldsymbol{x}_c) = \boldsymbol{u}_{FS}(\boldsymbol{x}_c, z_b), \tag{20}$$

provides the coupling to the FS solution. Here we take the $\boldsymbol{u}_{FS}$ at z_b, but any z can be chosen since $\boldsymbol{x}_c$ should be located such that $\boldsymbol{u}_{FS}(\boldsymbol{x}_c, z)$ hardly varies with z. Every iteration, $\boldsymbol{f}_{SSA}$ and $\boldsymbol{u}_{FS}(\boldsymbol{x}_c, z_b)$ are updated until convergence up to a tolerance ε_c.

3.2 Surface evolution

The surface evolution is calculated differently in the two domains Ω_{FS} and Ω_{SSA}. Equation (14) is applied to Ω_{FS} for the evolution of z_s and z_b, avoiding assuming hydrostatic equilibrium beyond the grounding line, since the flotation criterion is not necessarily fulfilled close to the grounding line (Durand et al., 2009). The thickness advection equation~~(~~, Eq. (15)~~)~~ , is used for Ω_{SSA}, which is advantageous since the ice flux $\boldsymbol{q} = H\boldsymbol{u}_{SSA}$ is directly available (because $\boldsymbol{u}_{SSA}$ does not vary with z) and no vertical velocity is needed. Moreover, only one time dependent equation is solved instead of one for the lower and one for the upper free surface. The evolution of the surfaces z_s and z_b for Ω_{SSA} is then calculated from the flotation criterion~~(~~, Eq. (12)~~). Equation (14) is applied to~~ . At $\boldsymbol{x}_c$, $H_{SSA} = H_{FS}$ is applied as a boundary condition to the thickness equation. First the surface evolution is solved for Ω_{FS}~~for the evolution of z_s and z_b, avoiding assuming hydrostatic equilibrium beyond the grounding line, since the flotation criterion is not necessarily fulfilled close to the grounding line (Durand et al., 2009), then~~ Ω_{SSA} follows.

3.3 The algorithm

The iterative coupling for one time step is given by Algorithm 1. First, the shortest distance d to the grounding line is computed for all nodes in the horizontal footprint mesh at the ice shelf base. Then, a mask is defined that describes whether a node is in Ω_{FS}, Ω_{SSA} or at the coupling interface $\boldsymbol{x}_c$, based on the user defined d_{GL}. Technically, the domain decomposition is based on the use of passive elements implemented in the overarching Elmer code (Råback et al., 2016), which allow for deactivating and reactivating of elements. An element in Ω_{FS} is passive for the SSA solver, which means that is not included in the global matrix assembly of $\mathbf{A}_{SSA}$, and vice-versa.

Two kinds of ~~iteration~~ iterations are involved, since computing either $\boldsymbol{u}_{FS,k}$ or $\boldsymbol{u}_{SSA,k}$ for the kth coupled iteration also requires Picard iteration by the non-linearity in ~~$\eta(\boldsymbol{u})$~~the viscosity. As the experiments will show, calculating $\boldsymbol{u}_{FS,k}$ dominates the computation time in the coupled model. The coupled model is therefore more efficient if the total number of FS Picard iterations (the sum of FS Picard iterations over all coupled iterations) decreases. This is accomplished by limiting the number of FS Picard iterations before continuing to compute $\boldsymbol{u}_{SSA,k}$, instead of continuing until the convergence tolerance ε_P is reached, since it is inefficient to solve very accurately for $\boldsymbol{u}_{FS,k}$ if the boundary condition at $\boldsymbol{x}_c$ is not yet accurate. Despite interrupting the Picard iteration, the final solution includes a converged FS solution since the coupled tolerance ε_c is reached. Picard iteration for $\boldsymbol{u}_{SSA,k}$ is always continued until convergence since the computation time is negligible compared to FS.

An element may switch from Ω_{SSA} to Ω_{FS}, for example during grounding line advance. Then, the coupled iteration either starts with the initial condition for $\boldsymbol{u}_{FS}$ if the element is in Ω_{FS} for the first time, or the latest $\boldsymbol{u}_{FS}(t)$ computed in this element, before switching to SSA.

Algorithm 1 Iteratively coupling FS and SSA for one time step, including surface update.

Initialize: $k := 0$, $\Omega := (\Omega_{FS}, \Omega_{SSA})$ by restricting Ω_{SSA} to the ice shelf and requiring $||\boldsymbol{x} - \boldsymbol{x}_{GL}||_h \geq d_{GL}$ for all $\boldsymbol{x}$ in Ω_{SSA}.

if $t > 0$ **then**

Take $\boldsymbol{u}_{FS,0}, \boldsymbol{u}_{SSA,0}, \boldsymbol{f}_{SSA,0}$ from previous time step.

else

$\boldsymbol{u}_{FS,0}, \boldsymbol{u}_{SSA,0}, \boldsymbol{f}_{SSA,0} = 0$.

end if

$converged$=false

while not $converged$ **do**

Compute $\boldsymbol{u}_{FS,k+1}$ on Ω_{FS} with boundary condition $\boldsymbol{\sigma}_{FS,k+1} \cdot \boldsymbol{n}(\boldsymbol{x}_c, z) = \rho g(z - z_s)\boldsymbol{n} + \frac{\boldsymbol{f}_{SSA,k}(\boldsymbol{x}_c)}{\omega H}$ at $\boldsymbol{x}_c$.

Compute $\boldsymbol{u}_{SSA,k+1}$ on Ω_{SSA} with boundary condition $\boldsymbol{u}_{SSA,k+1}(\boldsymbol{x}_c) = \boldsymbol{u}_{FS,k+1}(\boldsymbol{x}_c, z_b)$.

Let $\boldsymbol{f}_{SSA,k+1} = A_{SSA,k+1}\boldsymbol{u}_{SSA,k+1} - \boldsymbol{b}_{SSA,k+1}$.

$converged = ||\boldsymbol{u}_{FS,k+1} - \boldsymbol{u}_{FS,k}||/||\boldsymbol{u}_{FS,k}|| \leq \varepsilon_c$ **and** $||\boldsymbol{u}_{SSA,k+1} - \boldsymbol{u}_{SSA,k}||/||\boldsymbol{u}_{SSA,k}|| \leq \varepsilon_c$

$k := k + 1$.

end while

Surface evolution by free surface equations (Eq. (14) for Ω_{FS} ~~and~~ .

Surface evolution by thickness equation (Eq. (15)) for Ω_{SSA}, with $H_{SSA}(\boldsymbol{x}_c) = H_{FS}(\boldsymbol{x}_c)$.

4 Numerical experiments

To validate the coupled model, we first verify for a conceptual ice shelf ramp that solutions obtained with the coupled model resemble the FS velocity in 2D and 3D. Then the coupled model is applied to a 2D conceptual marine ice sheet (MIS). Whenever ~~*accuracy of the coupled model*~~ 'accuracy of the coupled model' is mentioned, this refers to the accuracy of the coupled model compared to the FS model. Investigating the accuracy of the FS model itself is outside ~~of~~ the scope of this study. No convergence study of the FS model with respect to discretization in either time or space is performed. Instead, equivalent settings are used for the FS and coupled model, such that they can be compared and the FS model is regarded as a reference solution.

4.1 Ice shelf ramp

4.1.1 Two dimensional ice shelf ramp

A simplified test case is chosen for which the analytical solution to the SSA equations exists in 2D as described in Greve and Blatter (2009). It consists of a 200 km long ice shelf (see Fig. 2), with a horizontal inflow velocity $u(0, z) = 100$ m yr^{-1} and a calving front at $x = 200$ km where the hydrostatic pressure as exerted by the sea water is applied. The shelf thickness linearly decreases from 400 m at $x = 0$ to 200 m at $x = 200$ km, z_b and z_s follow from the flotation criterion~~(~~, Eq. (12)~~)~~. By construction, the SSA model is expected to be a good approximation of the FS model. The domain is discretized by a structured

mesh, equidistant nodes on the horizontal axis, and extruded along the vertical to quadrilaterals. All constants used and mesh characteristics are specified in Table A1.

Three models are applied to this setup, FS-only, SSA-only, and the coupled model~~. The horizontal velocities computed by the models are denoted respectively~~, for which the horizontal velocities are denoted $u_{FS}, u_{SSA},$ and u_c respectively. The relative node-wise velocity differences between u_{SSA} and u_{FS} stay below 0.02% in the entire domain. However, computing time for the SSA solution only takes 3% of that of the FS solution, which is promising for the potential ~~speed up~~ speedup of the coupled model.

The coupling location is ~~defined in the middle of the domain (~~fixed at $x_c = 100$ km~~)~~, as no grounding line is present to relate x_c to. In the first coupled iteration, ~~the velocity at x_c is equal to the inflow velocity, $u_c(x_c, z_b) = 100$ m yr^{-1} compared to~~, while in the final solution $u_{FS}(x_c, z_b) = 4805$ m yr^{-1}. The cryostatic pressure applied to Ω_{FS} at x_c buttresses the ice flow completely and the force imbalance of the hydrostatic pressure at the calving front does not yet influence the velocity u_c in Ω_{FS}. ~~Already in~~ In the second iteration, when $\boldsymbol{f}_{SSA}$ is applied, a maximum difference of only 0.3% between u_{FS} and u_c in the entire domain remains. The coupling converges after three iterations, the velocity u_c and relative difference compared to FS are shown in Fig. 2. Convergence of the coupled model requires 31 FS Picard iterations compared to 35 for FS-only. However, ~~the coupled model needs almost twice as much computation time as the FS model, since~~ assembly time per FS iteration almost doubles in the coupled model compared to the FS model, and assembly time dominates the computational work in this simplified 2D case. Therefore, the coupled model needs almost twice as much computation time as the FS model. This issue is due to usage of passive elements and is addressed in the Discussion (Sect. 5).

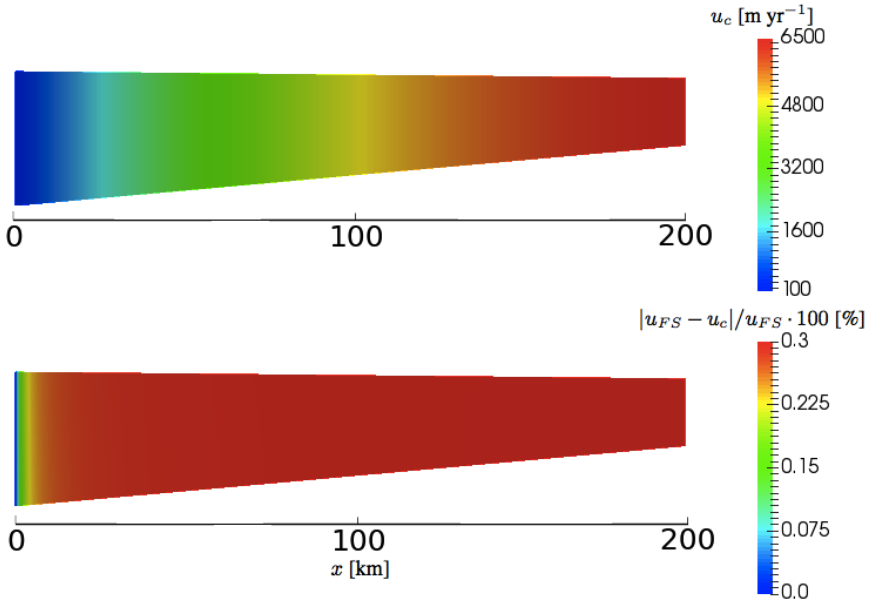

Figure 2. The horizontal velocity u_c [m yr^{-1}] and node-wise difference $|u_{FS} - u_c|/u_{FS} \cdot 100$ [%] in the coupled solution for the 2D ice shelf ramp. The vertical scale is exaggerated 100 times. The ice thickness ranges from 400 to 200 m.

4.1.2 Three dimensional ice shelf ramp

The 2D ice shelf ramp is extruded along the y-axis (see Fig. 3). On both lateral boundaries at $y = 0$ and 20 km, ~~$v = 0$ m yr^{-1}.~~ $\boldsymbol{u} \cdot \boldsymbol{n}$=0. All other boundary conditions remain identical to the 2D case and the coupling interface is located halfway $\boldsymbol{x}_c = (100, y)$ km. First the solutions of the FS and SSA model in Elmer/Ice will be compared before applying the coupled model.

The limited width of the domain (20 km) in combination with the boundary condition ~~$v = 0$ m yr^{-1}~~ $\boldsymbol{u} \cdot \boldsymbol{n} = 0$ at both lateral sides yields a negligible flow in the y direction ($v_{FS} < 10^{-8}$ m yr^{-1}). Despite differences in the models, the relative difference in u is below 1.5%. Running the experiment with the SSA model takes only 0.8% of the time needed to run it with the FS model.

The maximum relative difference between $\boldsymbol{u}_{FS}$ and $\boldsymbol{u}_c$ is 1.4%, which is of the same order of magnitude as the velocity difference between FS and SSA. The mean assembly time per FS iteration is 6% higher than in the FS-only model, but the solution time decreases by 55%. Convergence of the coupled model requires 30 FS iterations compared to 27 for FS-only. The total computation time decreases by 32%~~despite the slight increase in assembly time and number of FS iterations~~.

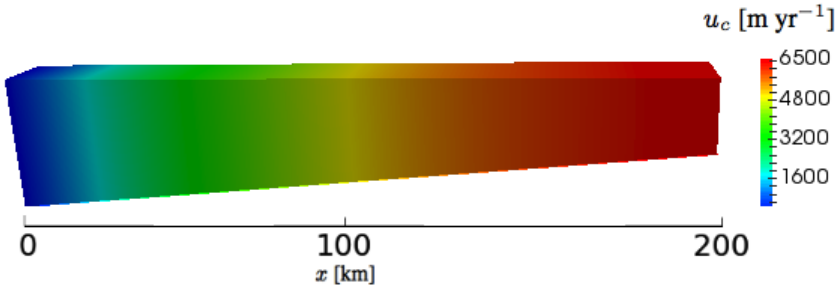

Figure 3. Horizontal velocity u_c [m yr^{-1}] from coupled model for the 3D ice shelf ramp ~~where~~ with $\boldsymbol{x}_c = (100, y)$ km.

4.2 Marine ice sheet

First, a diagnostic MIS experiment is performed in 2D to compare velocities for the initial geometry. After one time step, velocity differences between the coupled and FS models yield geometric differences. In prognostic experiments, velocity differences can therefore be due to the coupling and to the different geometry for which the velocity is solved. Computation times for the FS and coupled model are presented for the prognostic case only.

4.2.1 Diagnostic MIS experiment

The domain starts with an ice divide at $x = 0$, where $u = 0$, and terminates at a calving front at $x = L = 1800$ km. An equidistant grid with grid spacing $\Delta x = 3.6$ km is used. Other values of constants and mesh characteristics are specified in Table A2. Gagliardini et al. (2016) showed that resolving grounding line dynamics with a FS model requires very high mesh

resolution around the grounding line. However, Gladstone et al. (2017) showed that the friction law assumed in this study (see Sect. 2.2.1) reduces mesh sensitivity of the FS model compared to the Weertman friction law assumed in Gagliardini et al. (2016), allowing the coarse mesh used here. The bedrock [m] is negative below sea level and is given by

$$b(x) = 200 - 900\frac{x}{L}. \tag{21}$$

Basal melt is neglected and the surface accumulation a_s [m yr^{-1}] is a function of the distance from the ice divide,

$$a_s(x) = \frac{\rho_w}{\rho}\frac{x}{L}. \tag{22}$$

This experimental setup is almost equivalent to Gladstone et al. (2017), except for that they applied a buttressing force to the FS equations. It is possible to parametrize buttressing for the SSA equations as well through applying a sliding coefficient (Gladstone et al., 2012b). This was not done here as it may introduce a difference between the FS and SSA models that is unrelated to the coupling.

The diagnostic experiments are run on a steady state geometry computed by the FS model. First, the experiment 'SPIN' in Gladstone et al. (2017) is performed, starting from a uniform slab of ice (H=300 m)~~.~~, applying the accumulation in Eq. (22) for 40 kyr, such that a steady state is reached. The geometry yielded from these SPIN runs (which include buttressing) is used in simulations without buttressing until a new steady state (defined as a relative ice volume change below 10^{-5}) is reached. This removal of buttressing leads to grounding line retreat from 871.2 km to 730.8 km.

The velocity u_c for the final steady state geometry is given in Fig. 4, with $d_{GL} = 30$ km such that 58% of the nodes in the horizontal footprint mesh are located inside Ω_{SSA} ($\theta = 0.58$). The coupled model converges after 27 FS iterations on the restricted domain Ω_{FS}, compared to 24 Picard iterations in the FS model. The relative difference between u_{FS} and u_c is below 0.5% (Fig. 4), this small difference shows that ~~the minimal distance d_{GL} before applying SSA~~ $d_{GL} = 30$ km is sufficient. For ~~the used mesh resolution (see Table A2)~~this configuration, 4% of the FS nodes are located between x_{GL} and x_c ~~for~~ with $d_{GL} = 30$ km, hence decreasing d_{GL} does not affect the proportion of nodes in Ω_{FS} significantly~~, therefore~~. Therefore, d_{GL} is kept equal to 30 km for the prognostic experiment.

4.2.2 Prognostic MIS experiment

The prognostic experiment is aimed to verify model reversibility as in Schoof (2007). Starting from the steady state geometry, the ice temperature T is lowered over a period of 500 years from -10 °C to -30 °C and back according to

$$T(t) = -10(2 - \cos(2\pi t/500))\,^{\circ}\text{C for } 0 \leq t \leq 500 \text{ yr}. \tag{23}$$

~~the~~ The resulting change in ~~the fluidity parameter~~ $\mathcal{A}$~~(~~, see Eq. (4)~~), inducing~~ , induces a grounding line advance and retreat~~and so changing~~ , and changes Ω_{SSA} by Eq. (17). Afterwards, $T = -10$ °C for 2500 years. Mass balance forcing is kept constant throughout. The length of one time step is 1 yr.

The maximum difference between u_c and u_{FS} after 3000 years is 10 m yr^{-1}, shown in Fig. 5, corresponding to a relative difference of 1.6%. The time evolution of $x_{GL}, u_b(x_{GL}), H(x_{GL})$ and the grounded volume V_g are shown in Fig. 6 and Fig.

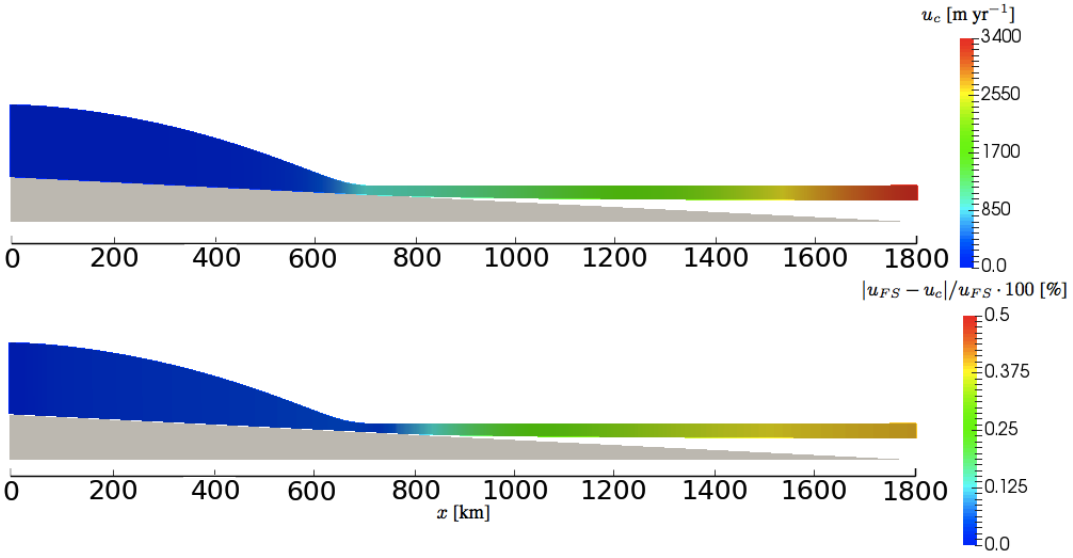

Figure 4. The coupled velocity u_c [m yr^{-1}] and relative difference $|u_{FS} - u_c|/u_{FS} \cdot 100$ [%], for the diagnostic MIS experiment. The bedrock is shaded in grey, $x_{GL} = 730.8$ km, $x_c = 763.2$ km (the mesh resolution yields $||\boldsymbol{x}_c - \boldsymbol{x}_{GL}||_h$=32.4 km). The vertical scale is exaggerated 100 times with an ice thickness ranging from 1435 m to 296 m.

7. In general, u_b is slightly higher in the coupled model, with a maximum difference of 5.3% in the entire experiment. The grounding line advances to $x_{GL} = 1036.8$ km in the FS model and $x_{GL} = 1044$ km in the coupled model. The FS model returns back to the original $x_{GL} = 730.8$ km, but the coupled model yields $x_{GL} = 734.4$ km, an offset of one grid point. The maximum difference in thickness is 1%. After 3000 years, V_g still decreases but the relative difference is below 10^{-5} between two time steps.

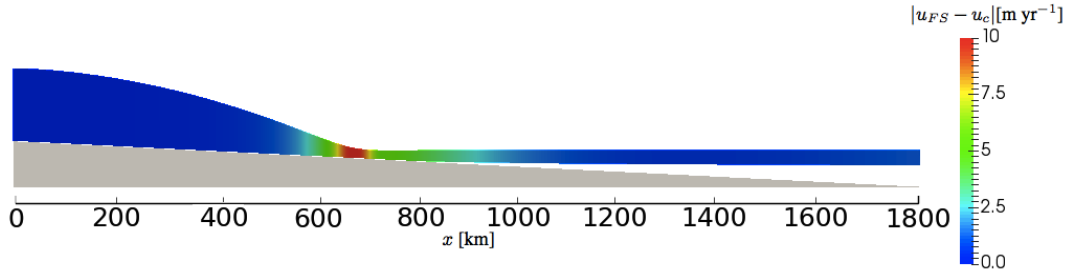

Figure 5. Absolute difference $|u_{FS} - u_c|$ [m yr^{-1}] after 3000 years. The vertical scale is exaggerated 100 times. The ice thickness ranges from 1445 m to 296 m.

To investigate efficiency of the coupled model, the simulation is performed with ten different settings, where the maximum number of FS iterations per coupled iteration is ~~limited~~ varied from one to ten. Assembly of the FS matrix takes 75% of

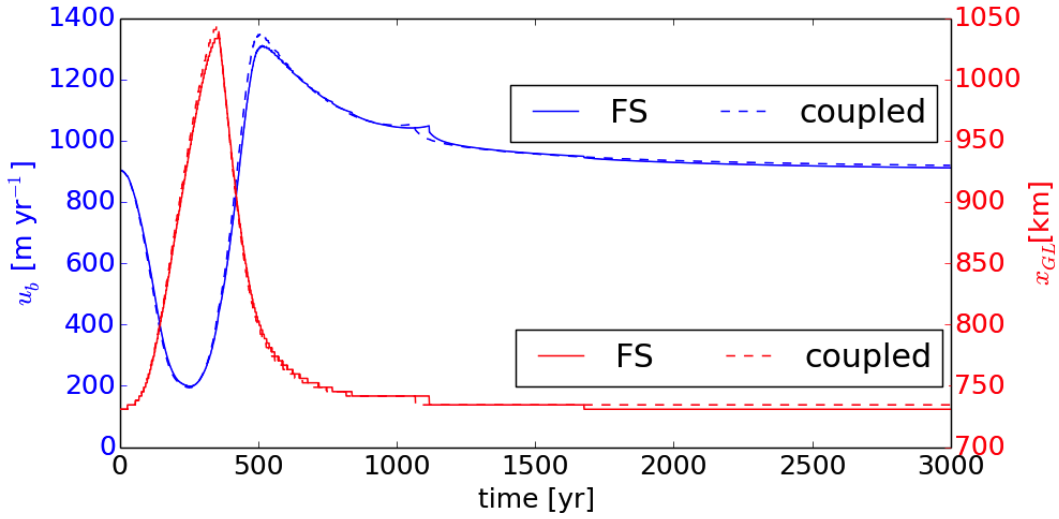

Figure 6. Time evolution of x_{GL} (red) and $u_b(x_{GL})$ (blue) with solid ~~line~~ lines for FS and dashed ~~line~~ lines for the coupled model.

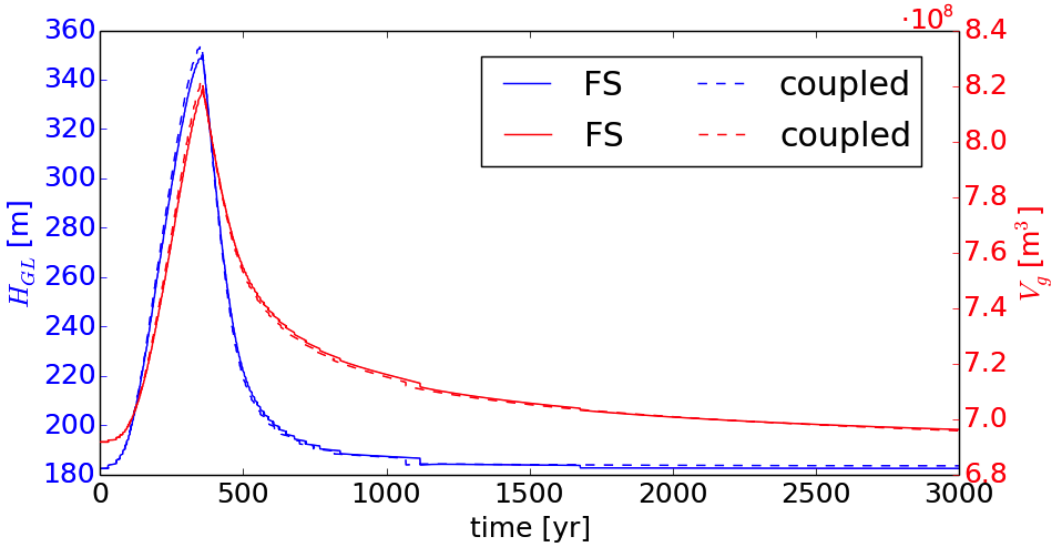

Figure 7. Time evolution of $H_{GL} = H(x_{GL})$ and grounded volume V_g with solid ~~line~~ lines for FS and dashed ~~line~~ lines for the coupled model.

the computation time of the FS model (see t_A in Table 1) and assembly time per FS iteration is similar for the coupled and FS model. Only 5% of the computation time is used to solve the linearized FS system ~~.~~ (t_s in Table 1). For all coupled simulations, assemblying and solving the SSA matrix (t_{SSA}) takes 4-6%. All time that is left will be called overhead, t_o, which includes launching solvers, i.e. allocating memory space for vectors and matrices, the surface evolution and solvers for post

model	t_A [%]	t_s [%]	# FS iter.	t_o [%]	t_{SSA} [%]	# coupled iter.	t_{tot} [cpu s]
FS	75	5	5.0	20	-	-	48641
C10	68	4	4.6	25	4	2.7	49724
C4	61	3	3.7	31	5	2.9	44143
C3	59	3	3.6	33	5	3.1	44040
C2	56	3	3.4	36	5	3.4	44334
C1	49	3	3.2	43	6	4.2	47135

Table 1. Computation times for MIS simulation of 3000 yr with FS-only and coupled model. Model Ci denotes the coupled model with i being the maximum number of non-linear FS iterations per coupled iteration, C5-C9 are omitted for brevity. The assembly time for $\mathbf{A}_{FS}$ is denoted t_A. All relative computation times are given in percentage of the total time t_{tot}. The number of FS and coupled iterations are averaged over the time steps.

processing. As expected, the total number of FS iterations is the smallest when just performing one FS Picard iteration per coupled iteration~~(on average 3.2 per time step)~~. However, the model then changes between solvers more often, meaning that ~~43% of computation time is used on overheads compared to 20% for the FS model and 25% for the coupled model with a limit of ten FS Picard iterations~~both overheads and the time to solve the SSA model increase. It turns out that a limit of three FS Picard iterations per coupled iteration balances minimizing ~~overhead and assembly time~~t_o and t_A, yielding a 10% decrease of computation time with respect to the FS model. This speedup ~~follows~~ comes from a lower number of FS Picard iterations (~~on average 3.6 per time step compared to 5 for the FS model~~Table 1) and a slight decrease of the time used to solve the linearized FS system (13% lower than the time that the FS model takes).

5 Discussion

The presented coupling is dynamic, since the coupling interface $\boldsymbol{x}_c$ changes with grounding line changes, but the distance d_{GL} ~~(~~that defines $\boldsymbol{x}_c$ ~~)~~ has to be chosen such that the FS velocity at the interface is ~~(almost)~~ almost independent of z. In the experiments described in Sect. ~~4,that~~ 4,this is already the case at the grounding line. We propose that further studies let Ω_{SSA} be determined automatically, for example ~~based on~~ by a tolerance for the vertical variation of the horizontal velocities~~(that~~, which should be close to zero in order to allow for a smooth coupling to SSA~~) or by using~~. Another option is to use a posteriori error estimates based on the residual ~~as derived in Jouvet (2016)~~(Jouvet, 2016).

~~Due to an inefficient matrix assembly, the~~ The current implementation in Elmer/Ice does not ~~allow for as much speed up~~ give as much speedup as expected from computation times of the FS- and SSA-only models for the ice shelf ramp ($t_{SSA} = 0.03 t_{FS}$) and from the performance estimates in Sect. ~~2.3.~~4.2.This is due to an inefficient matrix assembly. The assembly of the system matrix $\mathbf{A}_{FS}$ restricted to Ω_{FS} currently takes at least as much time as the assembly for the full domain Ω, even though the domain Ω_{FS} is much smaller than Ω~~(~~; in Eq. (~~16),~~13),$\theta = 0.5$ for the ice shelf ramp and and $\theta = 0.58$ for the diagnostic MIS experiment~~). This is problematic since~~ . Since the assembly time dominates the total solution time in simple

2D simulations, this is problematic. The inefficient assembly is caused by the use of passive elements implemented in the overarching Elmer code (Råback et al., 2016), which allow ~~for deactivating and reactivating~~ de- and reactivation of elements. A passive element is not included in the global matrix assembly, but every element must be checked to determine if it is passive. The inefficient assembly can be overcome by implementing the coupling on a lower level, hardcoded inside the FS solver~~, as~~ . This was done for the coupling of SIA and FS in ~~ISCAL (Ahlkrona et al., 2016)~~Ice Sheet Coupled Approximation Levels (ISCAL, see Ahlkrona et al., 2016), which showed significant ~~speed up~~ speedup when restricting the FS solver to a smaller domain. However, using passive elements is more flexible, since the coupling is independent of the solver used to compute velocities outside Ω_{SSA}. One is free to choose between the two different FS solvers in Elmer/Ice ~~(standard or block preconditioned, see Gag~~ (see Gagliardini et al., 2013) or to apply ISCAL. The latter is irrelevant in the experiments presented here since both the grounded and floating ice experiences low basal drag, and SIA is not capable of representing ice stream and shelf flow. Only a preliminary 3D experiment is performed here, since the current implementation is not sufficiently efficient to allow extensive testing in 3D. If the coupling is implemented efficiently such that the time spent on solving the FS equations on the restricted domain Ω_{FS} scales with the size of Ω_{FS}, the computational work ~~will~~ is expected to decrease significantly (see Sect. ~~2.3).~~4.2).

6 Conclusions

We have presented a novel FS-SSA coupling in Elmer/Ice, showing a large potential for reducing the computation time without losing accuracy. At the coupling interface, the FS velocity is applied as an inflow boundary condition to SSA. Together with the cryostatic pressure, a depth averaged contact force resulting from the SSA velocity is applied as a boundary condition for FS. The main finding of this study is that the two-way coupling is stable and converges to a velocity that is very similar to the FS model in the tests on conceptual marine ice sheets, and it yields a ~~speed up~~ speedup in 3D.

In diagnostic runs, the relative difference in velocity obtained from the coupled model and the FS model is below 1.5% when applying SSA at least 30 km seaward from the grounding line. ~~Also during~~ During a transient simulation, where the coupling interface changes dynamically with migration of the grounding line, the coupled model is very similar to the FS model, with a maximum difference of 5.3% in basal velocity at the grounding line. An offset of 3.6 km remains in the reversibility experiment in Sect.~~4.2.2,~~ 4.3, which is within the range of the expected resolution dependence for FS models (Gladstone et al., 2017).

In experiments involving areas where SIA is applicable, this new FS-SSA model can be combined with the ~~Ice Sheet Coupled Approximation Levels (ISCAL)~~ ISCAL method in Ahlkrona et al. (2016) ~~,~~ that couples SIA and FS in Elmer/Ice. This mixed model is motivated by paleo-simulations, but ~~combining~~ reducing computational work by the combination of multiple approximation levels is ~~in general useful for reduction of the computational work, for~~ also convenient for parameter studies, ensemble simulations, and inverse problems.

Code availability. The code of Elmer/Ice is available at https://github.com/ElmerCSC/elmerfem/tree/elmerice and can be redistributed and/or modified under the terms of the GNU General Public License as published by the Free Software Foundation; either version 2 of

the License, or (at your option) any later version. An example of the coupling is provided at https://github.com/ElmerCSC/elmerfem/tree/elmerice/elmerice/Tests/MISMIP_FS-SSA, which is also linked to the doi 10.5281/zenodo.1202407. Besides that, it is possible to access the version of the Elmer/Ice code including the coupling discussed in the paper, by using the SHA linked to the commit of the code, at https://github.com/ElmerCSC/elmerfem/archive/ba117583defafe98bb6fd1793c9c6f341c0c876.zip.

Appendix A: Derivation of the interface boundary condition

The boundary condition in Sect. 3.1 between the FS and the SSA domains is derived following a standard procedure in FEM using the weak formulation of the equations. Let $\Omega_{FS} \in \mathbb{R}^d$, $d = 2, 3$, denote the open FS domain in two or three dimensions with the boundary Γ_{FS}. After multiplying Eq. (2) with a test ~~funcion~~ function $\boldsymbol{v}$ and integrating over the domain Ω_{FS}, the weak form of Eq. (2) is

$$-\int_{\Omega_{FS}} \boldsymbol{v} \cdot (\nabla \cdot \boldsymbol{\sigma}) = \int_{\Omega_{FS}} \rho \boldsymbol{v} \cdot \boldsymbol{g}. \tag{A1}$$

Use the definition of $\boldsymbol{\sigma}$ and the divergence theorem to rewrite Eq. (A1),

$$\int_{\Omega_{FS}} \eta \mathbf{D}(\boldsymbol{u}) : \mathbf{D}(\boldsymbol{v}) - \int_{\Omega_{FS}} p \nabla \cdot \boldsymbol{v} = \int_{\Omega_{FS}} \rho \boldsymbol{v} \cdot \boldsymbol{g} + \int_{\Gamma_{FS}} \boldsymbol{v} \cdot \boldsymbol{\sigma} \cdot \boldsymbol{n}. \tag{A2}$$

The operation $\mathbf{A} : \mathbf{B}$ denotes the sum $\sum_{i,j} A_{ij} B_{ij}$. The test function $\boldsymbol{v}$ vanishes on the inflow boundary Γ_i, has a vanishing normal component on the bedrock boundary Γ_b, and lives in the Sobolev space $[W^{1,1/n+1}(\Omega_{FS})]^d$ (Jouvet, 2016), i.e.

$$\boldsymbol{v} \in \mathcal{V}_0 = \{\boldsymbol{v} \in [W^{1,1/n+1}(\Omega_{FS})]^d | \ \boldsymbol{v}|_{\Gamma_i} = 0, \ \boldsymbol{v}|_{\Gamma_b} \cdot \boldsymbol{n} = 0\}. \tag{A3}$$

The space $\mathcal{V}_0$ has this form because the boundary conditions on Γ_i and Γ_b are of Dirichlet type. ~~The boundary integral~~ Furthermore, there is a lateral boundary Γ_ℓ for $\Omega_{FS} \in \mathbb{R}^3$, where the normal component also vanishes: $\boldsymbol{v}|_{\Gamma_\ell} \cdot \boldsymbol{n} = 0$ and we assume a vanishing Cauchy-stress vector for unset boundary conditions to velocity components, such that the integral over Γ_ℓ vanishes. Then, the boundary integral in Eq. (A2) consists of a sum of the remaining boundary terms

$$\int_{\Gamma_{FS}} \boldsymbol{v} \cdot \boldsymbol{\sigma} \cdot \boldsymbol{n} = \sum_{i=1}^{d-1} \int_{\Gamma_b} f \boldsymbol{u} \cdot \boldsymbol{t}_i \boldsymbol{v} \cdot \boldsymbol{t}_i - \int_{\Gamma_w} p_w \boldsymbol{n} \cdot \boldsymbol{v} + \int_{\Gamma_{FSint}} \boldsymbol{v} \cdot \boldsymbol{\sigma} \cdot \boldsymbol{n}, \tag{A4}$$

given by the boundary conditions on Γ_b in Eq. (8) and (9), on the ocean boundary Γ_w in Eq. (13), and the internal boundary Γ_{FSint} between the FS and the SSA domains. The force $\boldsymbol{\sigma} \cdot \boldsymbol{n}$ on Γ_{FSint} is determined by the SSA solution.

The open SSA domain ~~$\Omega_{SSA} \in \mathbb{R}^{d-1}$~~ $\Omega_{SSA} \in \mathbb{R}^2$, coupled to $\Omega_{FS} \in \mathbb{R}^3$, has the boundary ~~$\Gamma_{SSA} = \Gamma_{SSAint} \cup \Gamma_{CF}$~~ $\Gamma_{SSA} = \Gamma_{SSAint} \cup$ where Γ_{SSAint} is adjacent to Ω_{FS} and partly coinciding with Γ_{FSint} (but of one dimension less) and Γ_{CF} is at the calving front. Let ~~$\mathbf{A}$~~ $\mathbf{B}$ have the elements

$$B_{11} = 4\bar{\eta}\frac{\partial u}{\partial x} + 2\bar{\eta}\frac{\partial v}{\partial y}, \ B_{12} = B_{21} = \bar{\eta}\frac{\partial u}{\partial y} + \bar{\eta}\frac{\partial v}{\partial x}, \ B_{22} = 2\bar{\eta}\frac{\partial u}{\partial x} + 4\bar{\eta}\frac{\partial v}{\partial y}, \tag{A5}$$

when $d = 3$. If $d = 2$, then ~~$A = 4\bar{\eta}\partial u/\partial x$~~ $B = 4\bar{\eta}\partial u/\partial x$. Then the SSA equations Eq. (6) can be written

$$\nabla_h \cdot \mathbf{A}\mathbf{B} = \boldsymbol{f}_g, \tag{A6}$$

where ~~$\boldsymbol{f}_g = \rho g H \nabla z_s$~~ and ~~$\nabla$~~ $\boldsymbol{f}_g = \rho g H \nabla_h z_s$ and ∇_h is the horizontal gradient operator. The boundary condition on Γ_{SSAint} is the Dirichlet condition, Eq. (20), and the force due to the water pressure at the calving front Γ_{CF} is $\boldsymbol{f}_{CF}$, as in Eq. (13) but integrated over z. Define the two test spaces

$$\mathcal{W} = \{\boldsymbol{v} \in [W^{1,1/n+1}(\Omega_{SSA})]^{d-1} | \ \boldsymbol{v}|_{\Gamma_\ell} \cdot \boldsymbol{n} = 0\}, \quad \mathcal{W}_0 = \{\boldsymbol{v} \in \mathcal{W} | \ \boldsymbol{v}|_{\Gamma_{SSAint}} = 0\}. \tag{A7}$$

Multiply Eq. (A6) by $\boldsymbol{v} \in \mathcal{W}_0$ and integrate. The weak form of Eq. (A6) is

$$\int_{\Omega_{SSA}} \boldsymbol{v} \cdot (\nabla_h \cdot \mathbf{A}\mathbf{B}) = \int_{\Omega_{SSA}} \boldsymbol{v} \cdot \boldsymbol{f}_g. \tag{A8}$$

Apply the divergence theorem to Eq. (A8) to obtain

$$-\int_{\Omega_{SSA}} \nabla_h \boldsymbol{v} : \mathbf{A}\mathbf{B} + \int_{\Gamma_{SSAint}\Gamma_{SSA}} \boldsymbol{v} \cdot \mathbf{A}\mathbf{B} \cdot \boldsymbol{n} = -\int_{\Omega_{SSA}} \nabla_h \boldsymbol{v} : \mathbf{A}\mathbf{B} + \pm \int_{\Gamma_{CF}} \boldsymbol{v} \cdot \boldsymbol{f}_{CF} + \int_{\Gamma_{SSAint}} \boldsymbol{v} \cdot \boldsymbol{f}_{SSA} = \int_{\Omega_{SSA}} \boldsymbol{v} \cdot \boldsymbol{f}_g. \tag{A9}$$

A mesh is constructed to cover Ω_{FS} and Ω_{SSA} with nodes at $\boldsymbol{x}_i$. In the finite element solution of Eq. (A9), the linear test function $\boldsymbol{v}_i \in \mathcal{W}_0$ is non-zero at $\boldsymbol{x}_i$ and zero in all other nodes. The integral over Γ_{SSAint} vanishes when $\boldsymbol{v} \in \mathcal{W}_0$. The finite element solution $\boldsymbol{u}_h$ of Eq. (A6) and (A9) satisfies

$$-\int_{\Omega_{SSA}} \nabla_h \boldsymbol{v}_i : \mathbf{A}\mathbf{B}(\boldsymbol{u}_h) + \int_{\Gamma_{CF}} \boldsymbol{v}_i \cdot \boldsymbol{f}_{CF} - \int_{\Omega_{SSA}} \boldsymbol{v}_i \cdot \boldsymbol{f}_g = 0, \ \boldsymbol{x}_i \in \Omega_{SSA} \cup \Gamma_{CF}. \tag{A10}$$

It follows from Eq. (A9) that with a test function $\boldsymbol{v}_i \in \mathcal{W}$ that is non-zero on Γ_{SSAint} and the solution $\boldsymbol{u}_h$ from Eq. (A10)

$$\int_{\Gamma_{SSAint}} \boldsymbol{v}_i \cdot \boldsymbol{f}_{SSA} = \tag{A11}$$

$$= \int_{\Omega_{SSA}} \nabla_h \boldsymbol{v}_i : \mathbf{B}(\boldsymbol{u}_h) - \int_{\Gamma_{CF}} \boldsymbol{v}_i \cdot \boldsymbol{f}_{CF} + \int_{\Omega_{SSA}} \boldsymbol{v}_i \cdot \boldsymbol{f}_g, \tag{A12}$$

$$\boldsymbol{x}_i \in \Omega_{SSA} \cup \Gamma_{CF} \cup \Gamma_{SSAint}. \tag{A13}$$

The first integral in Eq. (A12) corresponds to $(\mathbf{A}_{SSA}\boldsymbol{u}_{SSA})_i$ in Sect. 3.1 and b_{SSAi} to the second and third integrals. By Eq. (A10), the right hand side of Eq. (A12) vanishes for all ~~i~~ $\boldsymbol{x}_i$ in Ω_{SSA} and on Γ_{CF}, but for a node on the internal boundary, $\boldsymbol{x}_i \in \Gamma_{SSAint}$, the force $\boldsymbol{f}_{SSA}$ from the ice due to the state $\boldsymbol{u}_h$ in Ω_{SSA} is obtained. The internal pressure in the ice in Ω_{SSA} is assumed to be cryostatic as in Eq. (18). Since $\boldsymbol{f}_{SSA}$ in Eq. (A11) is integrated in the z direction over the thickness of the ice, the relation between $\boldsymbol{\sigma} \cdot \boldsymbol{n}$ in Eq. (A4) and $\boldsymbol{f}_{SSA}$ in Eq. (A11) is

$$\boldsymbol{\sigma} \cdot \boldsymbol{n} = H^{-1} \boldsymbol{f}_{SSA} - \rho g (z_s - z) \boldsymbol{n}, \tag{A14}$$

cf. Eq. (19). Thus, by computing the residual as in Eq. (19) the two finite element solutions in Ω_{FS} and Ω_{SSA} are coupled together at the common boundary Γ_{FSint} and Γ_{SSAint}.

Author contributions. NK, EvD, RvdW, MvG, PL, LvS designed the study. EvD implemented the coupling and carried out the numerical simulations, with support from TZ and CG. EvD drafted the manuscript with support from NK, and all authors contributed to the final version.

Competing interests. All other authors declare that they have no conflict of interest.

Acknowledgements. This work has been supported by FORMAS grant 214-2013-1600 to Nina Kirchner. Thomas Zwinger's contribution was supported by the Academy of Finland (grant number 286587). The computations were performed on resources provided by the Swedish National Infrastructure for Computing (SNIC) at PDC Center for High Performance Computing at KTH. We are grateful to Mika Malinen, Peter Råback and Juha Ruokolainen for advice in developing the coupling, to Rupert Gladstone for providing the setup as in Gladstone et al. (2017) and to Felicity Holmes, Guillaume Jouvet and Daniel Farinotti for their feedback on a draft of the manuscript. We wish to acknowledge the constructive comments of two anonymous reviewers, which contributed to improve the manuscript.

References

Ahlkrona, J., Lötstedt, P., Kirchner, N., and Zwinger, T.: Dynamically coupling the non-linear Stokes equations with the shallow ice approximation in glaciology: Description and first applications of the ISCAL method, J. Comput. Phys., 308, 1–19, 2016.

Alley, R. B., Clark, P. U., Huybrechts, P., and Joughin, I.: Ice-sheet and sea-level changes, Science, 310, 456–460, 2005.

Asay-Davis, X. S., Cornford, S. L., Durand, G., Galton-Fenzi, B. K., Gladstone, R. M., Gudmundsson, G. H., Hattermann, T., Holland, D. M., Holland, D., Holland, P. R., Martin, D. F., Mathiot, P., Pattyn, F., and Seroussi, H.: Experimental design for three interrelated marine ice sheet and ocean model intercomparison projects: MISMIP v. 3 (MISMIP+), ISOMIP v. 2 (ISOMIP+) and MISOMIP v. 1 (MISOMIP1), Geosci. Model Dev., 9, 2471–2497, doi:10.5194/gmd-9-2471-2016, 2016.

Baiocchi, C., Brezzi, F., and Franca, L. P.: Virtual bubbles and Galerkin-least-squares type methods, Comp. Meths. Appl. Mech. Engrg., 105, 125–141, 1993.

Benzi, M., Golub, G. H., and Liesen, J.: Numerical solution of saddle point problems, Acta Numer., 14, 1–137, 2005.

Bernales, J., Rogozhina, I., Greve, R., and Thomas, M.: Comparison of hybrid schemes for the combination of shallow approximations in numerical simulations of the Antarctic Ice Sheet, The Cryosphere, 11, 247–265, 2017.

Brondex, J., Gagliardini, O., Gillet-Chaulet, F., and Durand, G.: Sensitivity of grounding line dynamics to the choice of the friction law, J. Glaciol., 63, 854–866, 2017.

Budd, W., Keage, P., and Blundy, N.: Empirical studies of ice sliding, J. Glaciol., 23, 157–170, 1979.

Church, J. A., Clark, P. U., Cazenave, A., Gregory, J. M., Jevrejeva, S., Levermann, A., Merrifield, M. A., Milne, G. A., Nerem, R. S., Nunn, P. D., et al.: Sea level change, in: Climate Change 2013: The Physical Science Basis. Contribution of Working Group I to the Fifth Assessment Report of the Intergovernmental Panel on Climate Change, T. F. Stocker et al., pp. 1137–1216, Cambridge Univ. Press, 2013.

Durand, G., Gagliardini, O., De Fleurian, B., Zwinger, T., and Le Meur, E.: Marine ice sheet dynamics: Hysteresis and neutral equilibrium, J. Geophys. Res.-Earth, 114, 2009.

Gagliardini, O. and Zwinger, T.: The ISMIP-HOM benchmark experiments performed using the Finite-Element code Elmer, The Cryosphere, 2, 67–76, 2008.

Gagliardini, O., Zwinger, T., Gillet-Chaulet, F., Durand, G., Favier, L., De Fleurian, B., Greve, R., Malinen, M., Martín, C., and Råback, P.: Capabilities and performance of Elmer/Ice, a new-generation ice sheet model, Geosci. Model Dev., 6, 1299–1318, 2013.

Gagliardini, O., Brondex, J., Gillet-Chaulet, F., Tavard, L., Peyaud, V., and Durand, G.: Impact of mesh resolution for MISMIP and MISMIP3d experiments using Elmer/Ice, The Cryosphere, 10, 307–312, 2016.

Gillet-Chaulet, F., Gagliardini, O., Seddik, H., Nodet, M., Durand, G., Ritz, C., Zwinger, T., Greve, R., and Vaughan, D. G.: Greenland Ice Sheet contribution to sea-level rise from a new-generation ice-sheet model, The Cryosphere, 6, 1561–1576, 2012.

Gladstone, R. M., Lee, V., Rougier, J., Payne, A. J., Hellmer, H., Le Brocq, A., Shepherd, A., Edwards, T. L., Gregory, J., and Cornford, S. L.: Calibrated prediction of Pine Island Glacier retreat during the 21st and 22nd centuries with a coupled flowline model, Earth Planet. Sci. Lett., 333, 191–199, 2012a.

Gladstone, R. M., Payne, A. J., and Cornford, S. L.: Resolution requirements for grounding-line modelling: sensitivity to basal drag and ice-shelf buttressing, Ann. Glaciol., 53, 97–105, 2012b.

Gladstone, R. M., Warner, R. C., Galton-Fenzi, B. K., Gagliardini, O., Zwinger, T., and Greve, R.: Marine ice sheet model performance depends on basal sliding physics and sub-shelf melting, The Cryosphere, 11, 319–329, 2017.

Glen, J.: Experiments on the deformation of ice, J. Glaciol., 2, 111–114, 1952.

Greve, R. and Blatter, H.: Dynamics of ice sheets and glaciers, Springer Science & Business Media, 2009.

Helanow, C. and Ahlkrona, J.: Stabilized equal low-order finite elements in ice sheet modeling–accuracy and robustness, Computat. Geosci., pp. 1–24, 2018.

Hindmarsh, R.: A numerical comparison of approximations to the Stokes equations used in ice sheet and glacier modeling, J. Geophys. Res.-Earth, 109, 2004.

Hutter, K.: Dynamics of glaciers and large ice masses, Annu. Rev. Fluid Mech., 14, 87–130, 1982.

Hutter, K.: Theoretical glaciology: Material science of ice and the mechanics of glaciers and ice sheets, vol. 1, Springer, 1983.

Jakobsson, M., Nilsson, J., Anderson, L., Backman, J., Björk, G., Cronin, T. M., Kirchner, N., Koshurnikov, A., Mayer, L., Noormets, R., et al.: Evidence for an ice shelf covering the central Arctic Ocean during the penultimate glaciation, Nat. Commun., 7, 10 365, 2016.

Joughin, I., Smith, B. E., and Medley, B.: Marine ice sheet collapse potentially under way for the Thwaites Glacier Basin, West Antarctica, Science, 344, 735–738, 2014.

Jouvet, G.: Mechanical error estimators for shallow ice flow models, J. Fluid Mech., 807, 40–61, 2016.

Larour, E., Seroussi, H., Morlighem, M., and Rignot, E.: Continental scale, high order, high spatial resolution, ice sheet modeling using the Ice Sheet System Model (ISSM), J. Geophys. Res.-Earth, 117, 2012.

MacAyeal, D. R.: Large-scale ice flow over a viscous basal sediment: Theory and application to ice stream B, Antarctica, J. Geophys. Res.-Sol. Ea., 94, 4071–4087, 1989.

Morland, L.: Unconfined ice-shelf flow, in: Dynamics of the West Antarctic Ice Sheet, pp. 99–116, Springer, 1987.

Nilsson, J., Jakobsson, M., Borstad, C., Kirchner, N., Björk, G., Pierrehumbert, R. T., and Stranne, C.: Ice-shelf damming in the glacial Arctic Ocean: dynamical regimes of a basin-covering kilometre-thick ice shelf, The Cryosphere, 11, 1745, 2017.

Nowicki, S., Bindschadler, R. A., Abe-Ouchi, A., Aschwanden, A., Bueler, E., Choi, H., Fastook, J., Granzow, G., Greve, R., Gutowski, G., et al.: Insights into spatial sensitivities of ice mass response to environmental change from the SeaRISE ice sheet modeling project II: Greenland, J. Geophys. Res.-Earth, 118, 1025–1044, 2013.

Paterson, W.: The physics of glaciers, 1994.

Pattyn, F.: A new three-dimensional higher-order thermomechanical ice sheet model: Basic sensitivity, ice stream development, and ice flow across subglacial lakes, J. Geophys. Res.-Sol. Ea., 108, 2003.

Pattyn, F. and Durand, G.: Why marine ice sheet model predictions may diverge in estimating future sea level rise, Geophys. Res. Lett., 40, 4316–4320, 2013.

Pattyn, F., Schoof, C., Perichon, L., Hindmarsh, R., Bueler, E., De Fleurian, B., Durand, G., Gagliardini, O., Gladstone, R., Goldberg, D., et al.: Results of the marine ice sheet model intercomparison project, MISMIP, The Cryosphere, 6, 573–588, 2012.

Pattyn, F., Perichon, L., Durand, G., Favier, L., Gagliardini, O., Hindmarsh, R. C., Zwinger, T., Albrecht, T., Cornford, S., Docquier, D., et al.: Grounding-line migration in plan-view marine ice-sheet models: Results of the ice2sea MISMIP3d intercomparison, J. Glaciol., 59, 410–422, 2013.

Phillips, T., Rajaram, H., and Steffen, K.: Cryo-hydrologic warming: A potential mechanism for rapid thermal response of ice sheets, Geophys. Res. Lett., 37, 2010.

Rignot, E., Jacobs, S., Mouginot, J., and Scheuchl, B.: Ice-shelf melting around Antarctica, Science, 341, 266–270, 2013.

Ritz, C., Edwards, T. L., Durand, G., Payne, A. J., Peyaud, V., and Hindmarsh, R. C.: Potential sea-level rise from Antarctic ice-sheet instability constrained by observations, Nature, 528, 115, 2015.

Råback, P., Malinen, M., Ruokolainen, J., Pursula, A., and Zwinger, T.: Elmer Solver Manual, 2016.

Schoof, C.: Ice sheet grounding line dynamics: Steady states, stability, and hysteresis, J. Geophys. Res.-Earth, 112, 2007.

Schoof, C. and Hewitt, I.: Ice-sheet dynamics, Annu. Rev. Fluid Mech., 45, 217–239, 2013.

Seddik, H., Greve, R., Zwinger, T., Gillet-Chaulet, F., and Gagliardini, O.: Simulations of the Greenland Ice Sheet 100 years into the future with the full Stokes model Elmer/Ice, J. Glaciol., 58, 427–440, 2012.

Seddik, H., Greve, R., Zwinger, T., and Sugiyama, S.: Regional modeling of the Shirase drainage basin, East Antarctica: full Stokes vs. shallow ice dynamics, The Cryosphere, 11, 2213, 2017.

Seroussi, H., Ben Dhia, H., Morlighem, M., Larour, E., Rignot, E., and Aubry, D.: Coupling ice flow models of varying orders of complexity with the Tiling method, J. Glaciol., 58, 776–786, 2012.

Stokes, C. R., Tarasov, L., Blomdin, R., Cronin, T. M., Fisher, T. G., Gyllencreutz, R., Hättestrand, C., Heyman, J., Hindmarsh, R. C., Hughes, A. L., et al.: On the reconstruction of palaeo-ice sheets: recent advances and future challenges, Quaternary Sci. Rev., 125, 15–49, 2015.

Table A1. Numerical values of the constants used in the ice shelf ramp experiment. Since the shelf is afloat, there is no sliding at the base.

Parameter	Symbol	Value	Unit
Ice density	ρ	900	kg m^{-3}
Water density	ρ_w	1000	kg m^{-3}
Gravitational acceleration	g	9.81	m s^{-2}
Fluidity parameter	$\mathcal{A}$	10^{-16}	Pa^{-3} yr^{-1}
Number elements	N_z	10	
	N_x	120	
	N_y	10	
Picard convergence tolerance	ε_P	10^{-3}	
Coupled convergence tolerance	ε_c	10^{-4}	

Table A2. Numerical values of the constants for the MIS experiment.

Parameter	Symbol	Value	Unit
Ice density	ρ	910	kg m^{-3}
Water density	ρ_w	1000	kg m^{-3}
Gravitational acceleration	g	9.81	m s^{-2}
Sliding parameter	β	7 $\cdot 10^{-6}$	MPa m $^{-4/3}$ yr $^{1/3}$
Temperature	T	-10	$^\circ$ C
Number elements	N_z	11	
	N_x	500	
Picard convergence tolerance	ε_P	10^{-4}	
Coupled convergence tolerance	ε_c	10^{-4}	
Time step	dt	1	yr